Comprehensive study of the pentad bending triad region of germane: Positions, strengths, widths and shifts of lines in the 2 ν 2 , ν 2 + ν 4 and 2 ν 4 bands of 70 GeH 4 , 72 GeH 4 , 73 GeH 4 , 74 GeH 4 , 76 GeH 4

O.N. Ulenikov, O.V. Gromova, E.S. Bekhtereva, N.I. Raspopova, A.V. Kuznetsov, V. Boudon, C. Sydow, K. Berezkin, S. Bauerecker

Journal Pre-proof

Comprehensive study of the pentad bending triad region of germane: Positions, strengths, widths and shifts of lines in the $2\nu_2$; $\nu_2+\nu_4$ and $2\nu_4$ bands of $^{70}GeH_4$; $^{72}GeH_4$; $^{73}GeH_4$; $^{74}GeH_4$; $^{76}GeH_4$

O.N. Ulenikov, O.V. Gromova, E.S. Bekhtereva, N.I. Raspopova, A.V. Kuznetsov, V. Boudon, C. Sydow, K. Berezkin, S. Bauerecker

PII: S0022-4073(21)00019-4
DOI: https://doi.org/10.1016/j.jqsrt.2021.107526
Reference: JQSRT 107526

To appear in: *Journal of Quantitative Spectroscopy & Radiative Transfer*

Received date: 20 November 2020
Revised date: 15 January 2021
Accepted date: 15 January 2021

Please cite this article as: O.N. Ulenikov, O.V. Gromova, E.S. Bekhtereva, N.I. Raspopova, A.V. Kuznetsov, V. Boudon, C. Sydow, K. Berezkin, S. Bauerecker, Comprehensive study of the pentad bending triad region of germane: Positions, strengths, widths and shifts of lines in the $2\nu_2$; $\nu_2+\nu_4$ and $2\nu_4$ bands of $^{70}GeH_4$; $^{72}GeH_4$; $^{73}GeH_4$; $^{74}GeH_4$; $^{76}GeH_4$, *Journal of Quantitative Spectroscopy & Radiative Transfer* (2021), doi: https://doi.org/10.1016/j.jqsrt.2021.107526

Highlights

- Positions, strengths, widths and shifts of lines are recorded for the pentad bending triad of $^{M}GeH_4(M = 70, 72, 73, 74, 76)$
- Effective dipole moment parameters of the pentad bending triad of MGeH4 are determined
- List of 164220transitions is presented

Comprehensive study of the pentad bending triad region of germane: Positions, strengths, widths and shifts of lines in the $2\nu_2$, $\nu_2+\nu_4$ and $2\nu_4$ bands of $^{70}GeH_4$, $^{72}GeH_4$, $^{73}GeH_4$, $^{74}GeH_4$, $^{76}GeH_4$

O. N. Ulenikov[‡,a], O. V. Gromova[a], E. S. Bekhtereva[a], N. I. Raspopova[a], A. V. Kuznetsov[b], V. Boudon[b], C. Sydow[c], K. Berezkin[c], and S. Bauerecker[§,c]

[a] Research School of High–Energy Physics, National Research Tomsk Polytechnic University, Tomsk 634050, Russia;

[b] Laboratoire Interdisciplinaire Carnot de Bourgogne, UMR 6303 CNRS-Univ. Bourgogne Franche-Comté 9 Avenue Alain Savary, BP 47 870, F-21078 Dijon Cedex, France;

[c] Institut für Physikalische und Theoretische Chemie, Technische Universität Braunschweig, D - 38106, Braunschweig, Germany.

To be submitted to JQSRT

with 10 Figures, 6 Tables, Supplementary data, and 26 Manuscript pages

[‡]Correspondence and proofs to Prof. O. N. Ulenikov,

E-mail: Ulenikov@mail.ru

[§]Correspondence for experimental issues to Prof. S. Bauerecker,

E-mail: s.bauerecker@tu-bs.de

Abstract

The high resolution infrared spectra of GeH_4 in its natural abundance were recorded with a Bruker IFS125 HR Fourier transform infrared spectrometer at an optical resolution of 0.003 cm^{-1} and analyzed in the region of 1400–2000 cm^{-1} where the first bending overtone $2\nu_2$, $2\nu_4$ and combinational $\nu_2 + \nu_4$ bands are located. Ro–vibrational line positions and energies of the $^{70}GeH_4$ species were analysed for the first time and line positions and energies of the $^{72}GeH_4$ and $^{74}GeH_4$ species were improved considerably in comparison with the preceding studies. The numbers of 2316/2406/873/3007/2257 transitions with $J^{max} = 21/23/18/22/19$ of the $2\nu_2$ (A_1- and $E-$type sub–bands), $2\nu_4$ (A_1-, $E-$ and F_2-type sub–bands) and $\nu_2+\nu_4$ (F_1- and F_2-type sub–bands) bands of the $^{70}GeH_4$, $^{72}GeH_4$, $^{73}GeH_4$, $^{74}GeH_4$, and $^{76}GeH_4$ molecules were used in the joint weighted fit of experimentally assigned transitions with the Hamiltonian model which takes the resonance interactions between the seven, $(0200, A_1)$, $(0200, E)$, $(0101, F_1)$, $(0101, F_2)$, $(0002, A_1)$, $(0002, E)$ and $(0002, F_2)$, vibrational states into account. From our preceding studies 5563 hot band transitions were also taken into account. As the result of a joint fit, a set of 129 fitted parameters was obtained which reproduce the initial 16422 experimental (including "hot") transitions of five isotopologues with the $d_{rms} = 3.26 \times 10^{-4}$ cm^{-1}. A line strength analysis of the 1697 experimentally recorded transitions of all species was made by the fit of their line shapes with the Hartmann-Tran profile and 13 effective dipole moment parameters were obtained from the weighted fit which reproduce the initial experimental line strengths with the $d_{rms} = 3.4\%$. Self–broadening coefficients of 993 lines and self–shift coefficients of 674 lines were determined from the multi–spectrum analysis of these lines.

1 Introduction

This work is a continuation of the recent high–resolution study of different isotopologues of the germane molecule [1] – [3]. Knowledge of spectroscopic characteristics of different isotopologues of germane is important in many fields of science and

technology, such as high purity semi–conductor manufacturing, [4] – [5], chemical physics and astrophysics, [6] – [11], etc. One of the important problems of chemical physics is the precise determination of intramolecular multidimensional potential and dipole moment surfaces, which can be used in numerous applied investigations. This problem can be solved by semi–empirical methods, or on the basis of *ab initio* calculations. In both cases, knowledge of high accurate spectroscopic information not only about the main species (in our case, $^{74}GeH_4$), but also about all possible isotopologues is very important. So one can state that high accuracy of spectroscopic information about characteristics of spectral lines (both line positions, and line strengths and widths) of different isotopologues of a molecule is essential and timely.

Germane in a natural isotopic composition produces complex infrared spectra. Not less than five stable isotopologues exist in proper abundances with mass numbers of 70 (20.55 %), 72 (36.74 %), 73 (7.67 %), 74 (27.37 %) and 76 (7.67 %). Additional complexity of the germane spectra arises from strong Coriolis interactions between the ν_2/ν_4 and ν_1/ν_3 pairs of its fundamentals. Germane is a spherical top molecule, and, as a consequence, it has no permanent dipole moment, and the possibilities of the ground state combination differences (GSCD) method (which was efficiently used by the authors in the study of molecules of other types, see, *e.g.*, Refs. [12] – [16]) are very limited as applied to germane.

In the present work we focus on the study of positions, strengths, line widths and pressure shifts of different isotopologues of germane in the region of their $2\nu_2$, $\nu_2 + \nu_4$ and ν_4 bands. Earlier high resolution spectra of germane have been studied in many laboratory investigations ([17]–[31] and references therein; see also recent quantitative study of line positions and strengths of the Dijon group, [32], with the resulting line lists included in the VAMDC/GeCaSDa database [33] and to be also inserted in the next HITRAN update, as a new molecule for this database). As to the spectral region considered in the present study, line positions in the $2\nu_2$, $\nu_2 + \nu_4$

and $2\nu_4$ bands were discussed earlier in [1] – [3] where specially enriched $^{76}GeH_4$ [1], $^{73}GeH_4$ [2] and $^{72}GeH_4$ [3] species have been analysed. In this case, line positions of the discussed absorption bands of $^{70}GeH_4$ and $^{74}GeH_4$ were not discussed earlier (in [1] the ro–vibrational structure of the $(0101, F_1)$ and $(0101, F_2)$ vibrational states was obtained from "hot" transitions). To our knowledge, experimental line strengths, widths and line shifts of germane in the region of its pentad bending triad were not discussed earlier at all for all isotopologues.

2 Experimental

The used GeH4 sample gas was purchased from Linde with a declared purity of 99.999%. This indicated purity was verified by three freeze–pump–thaw cycles. As germane is a highly flammable, potentially pyrophoric/self–igniting and highly toxic gas [34], precautions have to be taken. So before inlet into the optical cell, a limited gas amount was prefilled in a 1000 ml bowl flask within a fume cupboard. The closed filling system for the optical measuring cells was flushed with nitrogen immediately after spectra recording, also compare [35].

For the present work, seven spectra of mono–germane in natural composition, GeH_4, have been recorded in our Braunschweig infrared laboratory in the spectral range of 600 – 4800 cm^{-1} (mostly 1400 – 2700 cm^{-1}) with a Bruker IFS125HR Fourier transform infrared spectrometer (Zürich prototype ZP2001 [36], see Table 1 for detailed conditions. The first spectrum has been recorded with a stainless–steel White cell with a base length of 1 m at the optical pathlength of 24.0524 ± 0.012 m and further six spectra were recorded with a one–path stainless–steel cell at the optical pathlength of 230.5 ± mm, all in combination with a MCT313 semiconductor detector. Further, a globar radiation source and a KBr beamsplitter were used at 0.003 cm^{-1} optical resolution and self–apodization (Boxcar). Between 300 and 1400 scans have been averaged, see Table 1.

For line strength determination, the accurate sample pressure is needed, so we used a cascade of three temperature compensating Pfeiffer capacitance sensor gauges in ceramic technology (CMR 361, CMR 362, and CMR 363), which are resistant against aggressive gaseous media and independent on the type of gas. Here, we used the first two with the ranges of 0.1 – 1100 hPa and 0.01 – 110 hPa. The manufacturer claims an accuracy on the measured value of 0.2 % so that we estimate the total errors of the sample pressures to be in the range of ±0.5% during the whole time spans of the presented experiments. The temperature was in the range of 23.4^{o}C to 23.8^{o}C with a deviation within a single measurement of up to ±0.7^{o}C, compare Table 1. It was monitored with a PT100 resistance thermometer, Ahlborn Almemo 2590, which has a stated accuracy of ±0.03% on the measured value.

The line strength S can be derived from the area of a single absorption line A_{Line} using the Beer–Lambert law, the pressure P of the pure gaseous species (GeH_4), the temperature T and the optical pathlength L:

$$S = \frac{k_B T}{PL} A_{\mathrm{Line}}, \tag{1}$$

where

$$A_{\mathrm{Line}} = \frac{1}{\log(\mathrm{e})} \int \log\left(\frac{I_0(\nu)}{I(\nu)}\right) d\nu. \tag{2}$$

.

The line intensities can be obtained by direct integration of the measured effective line absorbance, which can be fitted well by a Voigt profile or a Hartmann–Tran line profile (as in the present work; compare line strength analysis in the following Sections). At 1750 cm^{-1} and room temperature the Doppler broadening for $^{74}GeH_4$ (the most abundant isotopologue of mono germane) is 0.0024 cm^{-1} and the instrumental line width is 0.0020 cm^{-1} at the adjusted optical resolution of 0.003 cm^{-1} in combination with boxcar apodisation. The full pressure widths for the seven spectra in the order of Table 1 are 0.00045 (0.0032), 0.0036 (0.0048), 0.0072 (0.0079), 0.0108

(0.0113), 0.0162 (0.0165), 0.0216 (0.0218), 0.0270 (0.0272) in cm^{-1}. The numbers in brackets are the total line widths which are approximated here by the root sum square of the convolution of Doppler, pressure and instrumental line widths which is in accordance with the experimental results. One can see that from the second pressure value of 20 hPa on, the pressure width is dominating the total line width increasingly with the pressure.

3 Assignment of transitions of the $^{70}GeH_4$, $^{72}GeH_4$ and $^{74}GeH_4$ species

As the first step of the present analysis, we performed an assignment of transitions of the $^{70}GeH_4$, $^{72}GeH_4$ and $^{74}GeH_4$ species in the studied spectra. For the convenience of the reader two overview spectra I and IIa which have been recorded under different experimental conditions, are shown in the upper traces of Figs. 1 and 2. For illustration of the quality of the recorded spectra, small parts of the high resolution spectrum IIa (for the stronger $\nu_2 + \nu_4$ band) and I (for the weaker $2\nu_2$ and $2\nu_4$ bands) are shown in Figs. 3 – 6 where clusters belonging to different isotopic species are marked.

For the assignment of transitions, the ground state parameters from Ref. [37] were used. As the result of the analysis, we assigned 3007 transitions with the value J^{max} = 22 to the $^{74}GeH_4$ species, 2406 transitions with the value J^{max} = 23 to the $^{72}GeH_4$ species, and 2316 transitions with the value J^{max} = 21 to the $^{70}GeH_4$ species (for details, see statistical information in Table 2). The full list of assigned transitions is presented as the Supplementary data 1 to this paper.

4 Joint ro-vibrational analysis of the pentad bending triad of five, $^{70}GeH_4$, $^{72}GeH_4$, $^{73}GeH_4$, $^{74}GeH_4$, and $^{76}GeH_4$ isotopologues of germane

The information on 6873 transitions obtained in the present study and discussed in Section 3 was added to the known information about the pentad bending triad and "hot" transitions of $^{72}GeH_4$, $^{73}GeH_4$, $^{74}GeH_4$, and $^{76}GeH_4$ from Refs. [1] – [3] (for details, see statistical information in Table 2), and both used then in the joint weighted fit of parameters of the effective rotational Hamiltonian,

$$\begin{aligned} H^{vib.-rot.} &= \sum_{v\gamma,v'\gamma'} \sum_{n\Gamma} [(|v\gamma\rangle \otimes \langle v'\gamma'|)^{n\Gamma} \otimes H^{n\Gamma}_{v\gamma,v'\gamma'}]^{A_1} \\ &\equiv \sum_{v\gamma,v'\gamma'} \sum_{n\Gamma} \sum_{\Omega K} [(|v\gamma\rangle \otimes \langle v'\gamma'|)^{n\Gamma} \otimes R^{\Omega(K,n\Gamma)}]^{A_1} Y^{\Omega(K,n\Gamma)}_{v\gamma,v'\gamma'}. \end{aligned} \quad (3)$$

Here $|v\gamma\rangle$ are symmetrized vibrational functions; $Y^{\Omega(K,n\Gamma)}_{v\gamma,v'\gamma'}$ are spectroscopic parameters; and $\otimes$ denotes a tensorial product. In this case, when $v = v'$ and $\gamma = \gamma'$, the parameters $Y^{\Omega(K,n\Gamma)}_{v\gamma,v\gamma}$ describe the rotational structure of the vibrational state $(v\gamma)$. If $\gamma = \gamma'$, but $v \neq v'$, the parameters $Y^{\Omega(K,n\Gamma)}_{v\gamma,v'\gamma}$ describe Fermi–type interactions. If $\gamma \neq \gamma'$ (v and v' are arbitrary), the parameters $Y^{\Omega(K,n\Gamma)}_{v\gamma,v'\gamma'}$ describe Coriolis–type interactions. The operators $R^{\Omega(K,n\Gamma)}_{\sigma}$ in Eq. (3) are determined as

$$R^{\Omega(K,n\Gamma)}_{\sigma} = \sum_{m} {}^{(K)}G^{m}_{n\Gamma\sigma} R^{\Omega(K)}_{m}, \quad (4)$$

where $R^{\Omega(K)}_{m}$ are the so–called irreducible rotational operators of the $SO(3)$ symmetry group, [38] – [41]; and the reduction matrix elements ${}^{(K)}G^{m}_{n\Gamma\sigma}$ are determined by the specific point symmetry group. Speaking about molecules of the T_d symmetry group, the numerical representation of the ${}^{(K)}G^{m}_{n\Gamma\sigma}$ values can be found in [42, 43, 44].

The following strategy was used in the fit of the Hamiltonian parameters. The values of all 16422 transitions (including "hot" transitions)obtained in the present study (see Section 3) and taken from [1] – [3] were used as the initial experimental data in the fit procedure. High order centrifugal distortion, tetrahedral splitting

and resonance interaction parameters which have been obtained in [1] – [3] from the large amount of experimental data for the $^{76}GeH_4$, $^{73}GeH_4$ and $^{72}GeH_4$ isotopologues were constrained to the values of corresponding parameters from [1] – [3] for all five isotopologues and were not varied during the fit. Such parameters are presented in Table 3 without confidence intervals (in Table 3, the latter are shown in parenthesis for the fitted parameters). All the other parameters were fitted by the usual procedure with the computer code SPHETOM of Tomsk Polytechnic University. After that (for the convenience of readers because they are more familiar with the Dijon STDS computer code [45] than with the SPHETOM code), values of all obtained parameters were transformed (re–fitted with the Dijon STDS code) to the values of corresponding parameters of the Dijon STDS format (about connection between the SPHETOM and Dijon STDS parameters, see, e.g., Ref. [46]). The final values of parameters of the triad bending states are presented (just in the Dijon STDS format) in Table 3 together with their 1σ statistical confidence intervals which are shown in parenthesis. For the convenience of the reader, parameters being necessary for calculation of the ground state and of the bending dyad are shown in Table 4 (parameters both from Table 3 and Table 4 can be directly used in the Dijon STDS code). From comparison of the parameters of the same label for different isotopologues one can make the conclusion that the obtained results are physically suitable. In particular, for any fitted parameter the condition is fulfilled that the value of a parameter, as a function of the mass of the Ge–nuclei, practically linearly depends on the value of this mass (this condition is one of the main conclusions of the isotopic substitution theory, [47], for the GeH_4-type molecules). The correctness of the result is confirmed by the good reproduction of the initial experimental line positions of both the "cold" and "hot" transitions by the set of 129 fitted parameters from Table 3: the general $d_{\rm rms}$ value for the whole set of 16422 transitions (both "cold" and "hot") is 3.26×10^{-4} cm^{-1} (for more detailed statistical information on the different bands of different isotopologues, see Table 2). For the "cold" bands of the $^{70}GeH_4$, $^{72}GeH_4$ and $^{74}GeH_4$ species which have been analysed in the present study for the first time, Figs. 7a – 7c show the (observed – calculated) line positions

and fit statistics.

5 Line strengths: Brief theoretical background

The theory of the line strength analysis of spherical top molecules on the basis of the Irreducible Tensorial Sets theory (ITST) was derived in [48] (see also [49]). In this section we very briefly present some basic relations necessary for the further analysis.

In the absence of external fields the intensity of the vibration–rotation line, due to transitions from the $|A\rangle$ to $|B\rangle$ state, is determined by the expression (see., e. g., [50]):

$$S_{\nu_0} = \frac{8\pi^3\nu_0}{4\pi\epsilon_0 3hc}\left[1-\exp\left(-\frac{hc\nu_0}{k_BT}\right)\right]N\frac{g_A}{Z(T)}\exp\left(-\frac{E_A}{k_BT}\right)\mathscr{R}_A^B, \tag{5}$$

where $\nu_0 = (E_B - E_A)/hc$ is the wavenumber of the transition, and E_B and E_A are the upper and the lower ro-vibrational energies of the transition; g_A is the nuclear spin statistical weight (for the GeH_4 molecule $g_A = 5$, 5, 2, 3, and 3 for the ro–vibrational states of the A_1, A_2, E, F_1, and F_2 symmetry, respectively, Ref. [51]). The value $Z(T)$ is the partition function. In the present study we used $Z(296.75) = 1724.46$ for the $^{74}GeH_4$ species which has been calculated with the formula from Ref. [52]. In general case, for the other temperatures, the partition function $Z(T)$ can be easily determined by the formula:

$$\begin{aligned} Q(T) \quad &= Q_v(T)\times Q_r(T) = \sum_v \exp\left(-\frac{hcE_v}{kT}\right) \\ &\times\left(\frac{27}{4}\right)\pi^{1/2}\left(\frac{kT}{hcB_{gr.}}\right)^{3/2}\exp\left(\frac{hcB_{gr.}}{4kT}\right), \end{aligned} \tag{6}$$

which is reproduced from Ref. [52] and valid for the molecules of the XH_4 (T_d symmetry) type with an accuracy no worse than 1 % (in Ref. [52] the notation $Q(T)$ is used for the partition function instead of $Z(T)$). For the calculation of the partition function $Z(T)$, the value of $B_{gr.} = 2.695864734$ cm^{-1} has been taken from Ref. [37]. Analogously, partition functions were obtained for the four other species of germane.

The according results are shown in the last line of Table 5.

The value $\mathscr{R}_A^B = |\langle A|\mu'_Z|B\rangle|^2$ in Eq. (5) is the matrix element of the operator

$$\mu'_Z = G^+ P_Z G \tag{7}$$

on the functions $|A\rangle$ and $|B\rangle$ of the lower and upper ro–vibrational states. The value P_Z is the $Z-$component of the dipole moment of a molecule (see, e.g., [53], [54]) and, depending on the instantaneous distances between nuclei, it can be written as

$$P_Z = \sum_\alpha k_{Z\alpha} \left(\mu_\alpha^e + \sum_\lambda \mu_\alpha^\lambda q_\lambda + \sum_{\lambda,\nu\geq\lambda} \mu_\alpha^{\lambda\nu} q_\lambda q_\nu + ... \right). \tag{8}$$

Here $k_{Z\alpha}$ are elements of the direction cosines matrix, Ref. [55]; μ_α^e are the components of the equilibrium (permanent) dipole moment of the molecule in the molecular–fixed coordinate system; q_λ are dimensionless normal vibrational coordinates, Refs. [56]–[57], of a molecule; and μ_α^λ, $\mu_\alpha^{\lambda\nu}$, ... are the parameters which describe the dependence of dipole moment components μ_α on the normal vibrational coordinates. The first terms (μ_α^e in Eq. (8)) are responsible for the pure rotational transitions; the second terms (which are proportional to the first order of vibrational coordinates) are responsible for the appearance of the fundamental band transitions in absorption (in more general case, of the bands which correspond to a change of only one vibrational quantum number by unit), etc. The operator G which is presented in Eq. (7) is an unitary operator known from the theory of effective operators (see, *e.g.*, Refs. [56]–[67]). If one takes the results of the mentioned articles into account, then it is possible to show that for an arbitrary polyatomic molecule Eq. (7) can be transformed to the following expression

$$\mu'_Z = \sum_v |0\rangle {}^v\mu_Z \langle v|, \tag{9}$$

where the values ${}^v\mu_Z$ depend only on the operators $k_{Z\alpha}$ and J_α and do not depend on the vibrational operators; $|0\rangle$ and $\langle v|$ are the vibrational function of the lower (in our case, of the ground) and upper vibrational states. In this case, the operators

${}^{v}\mu_Z$ have the following form:

$$ {}^{v}\mu_Z = \sum_j {}^{v}\mu_j {}^{v}A_j, \tag{10} $$

and ${}^{v}\mu_j$ and ${}^{v}A_j$ are called as the effective dipole moment parameters of a specific vibrational band, $\langle v| \leftarrow |0\rangle$, and symmetrized rotational operators.

It is well known (see, e.g., [40, 41], [68]–[70]), that the ro–vibrational spectroscopic study of the XY_4 (T_d) molecules is most efficient if one uses a special mathematical formalism of the irreducible tensorial sets theory (ITST), [71]–[73]. The boggest advantage of the ITST use consists in the possibility to replace the calculation of numerous matrix elements of different operators by combinations of simple and well–known values, such as Clebsch–Gordan coefficients, 3Γ and 6Γ symbols of the SO(3) and of point symmetry (in our case, T_d-symmetry) groups and of so–called G–reduction matrixes. For the T_d-symmetry molecules all of these coefficients are well known (see, e.g., Refs. [55], [69], [74]–[75]), and they can be easily used for calculation of the matrix elements $\mathscr{R}_A^B$ in Eq. (5) on the basis of formulas, Eqs. (6) – (10). All the above formulas should be adapted to ITST notations. In particular, it is possible to show that the formula, Eq. (9), can be transformed to the following expression [49]:

$$ \left(\mu'_z\right)^{\Gamma} = \sum_{\substack{v_1 l_1 \Gamma_1 \\ v_2 l_2 \Gamma_2}} \left([|v_1 l_1 \Gamma_1\rangle \otimes \langle v_2 l_2 \Gamma_2|]^{(\Gamma \otimes \Gamma_r)} \otimes R^{\Omega K(\tilde{K}, n\Gamma_r)} \right)^{\Gamma} P^{\Omega K(\tilde{K}, n\Gamma_r)}_{v_1 l_1 \Gamma_1, v_2 l_2 \Gamma_2}. \tag{11} $$

In Eq. (11), the $|v_1 l_1 \Gamma_1\rangle$ and $\langle v_2 l_2 \Gamma_2|$ are the symmetrized vibrational functions (v and l are vibrational quantum numbers, Γ is the symmetry of the function); $P^{\Omega K(\tilde{K}, n\Gamma_r)}_{v_1 l_1 \Gamma_1, v_2 l_2 \Gamma_2}$ are the parameters of the effective dipole moment operator for the band $(v_2 l_2 \Gamma_2) \leftarrow (v_1 l_1 \Gamma_1)$; $R^{\Omega K(\tilde{K}, n\Gamma_r)}$ are the symmetrized rotational operators (for more details, see [48], [49]); and the symbol $\otimes$ denotes the direct product, [72].

Finally, for calculation of the matrix elements $\mathscr{R}_A^B$ in Eq. (5), it is necessary to have ro–vibrational functions $|A\rangle$ and $|B\rangle$. For the XY_4 (T_d) molecules, it is clearly logical to take functions which are symmetrized on the basis of ITST. Such ro–vibrational

functions can be taken in the following form:

$$|A\rangle_s^C = |vl\Gamma; Jn\gamma^r; CS\rangle = [|vl\Gamma\rangle \otimes |Jn\gamma^r\rangle]_s^C \,, \tag{12}$$

where $|Jn\gamma^r\rangle$ is the rotational function of the γ^r symmetry and C is the symmetry of a function of the ro–vibrational state.

In the further analysis, Eqs. (11) and (12) were used for calculation of the matrix elements $\langle v_1 l_1 \Gamma_1; J_1 n_1 \gamma_1^r; C_1 s_1 | \left(\mu_z'\right)^\Gamma | v_2 l_2 \Gamma_2; J_2 n_2 \gamma_2^r; C_2 s_2 \rangle$ which are necessary for determination of the values $\mathscr{R}_A^B$ in Eq. (5).

6 Line strengths: Analysis of the $2\nu_2/\nu_2 + \nu_4/2\nu_4$ bending triad of germane: The $^{70}GeH_4$, $^{72}GeH_4$, $^{73}GeH_4$, $^{74}GeH_4$ and $^{76}GeH_4$ species

For the line strength analysis of the $\nu_2 + \nu_4(F_2)$ and $\nu_2 + \nu_4(F_1)$ bands, spectrum IIa (see Fig. 2) was used. The line strength analysis of the considerably weaker $2\nu_2$ and $2\nu_4$ bands was made with spectrum I (see Fig. 1). Spectrum I was also used for the strength analysis of transitions of the $\nu_2 + \nu_4$ band which correspond to high values of the quantum number J. The 1697 unblended nonsaturated and not too weak ro–vibrational lines have been chosen in these two experimental spectra (see column 5 of the Supplementary data 2): 382, 511, 116, 556 and 132 for the $^{70}GeH_4$, $^{72}GeH_4$, $^{73}GeH_4$, $^{74}GeH_4$ and $^{76}GeH_4$ species, respectively (line positions in column 3 of the Supplementary data 2 are reproduced from Refs. [1, 2] and from the Supplementary data 1 of the present paper). Integrated intensities of these lines were obtained from the fit of their line shapes. A box–car apodization line shape function, [36], [76], and the Hartmann–Tran profile of individual ro–vibrational transition, Refs. [77] – [78], which have been recommended recently for description of isolated high–resolution spectroscopic transitions, Refs. [79], were used in the fit. The Hartmann–Tran profile function is based on the binary collision model, Ref. [80], has the following

form, Ref. [79]:

$$F_{HTP}(\nu) = \frac{1}{\pi}\mathtt{Re}\left\{\frac{A(\nu)}{1-[\nu_{\rm vc}-\eta(C_0-3C_2/2)]A(\nu)+\left(\frac{\eta C_2}{\nu_{a0}^2}\right)B(\nu)}\right\} \tag{13}$$

and generalizes many of the precursor profile models (see, *e.g.*, Voigt, Refs. [81] – [83]; Rautian, Ref. [84]; speed–dependent Voigt, Refs. [85] – [86]; speed–dependent Rautian, Ref. [87], *etc.*, being one of the speed depended models, see, *e.g.*, Refs. [88] – [94]), the Hartmann – Tran profile allows one to take into account collisional narrowing for isolated spectral lines). In Eq. (13) it is denoted (with notations reproduced from [79]):

$$A(\nu) = \frac{\sqrt{\pi}c}{\nu_0\nu_{a0}}[\omega(iZ_-)-\omega(iZ_+)] \tag{14}$$

and

$$B(\nu) = \frac{\nu_{a0}^2}{\tilde{C}_2}\left[-1+\frac{\sqrt{\pi}}{2\sqrt{Y}}(1-Z_-^2)\omega(iZ_-)-\frac{\sqrt{\pi}}{2\sqrt{Y}}(1-Z_+^2)\omega(iZ_+)\right], \tag{15}$$

where

$$\omega(z) = \frac{i}{\pi}\int_{-\infty}^{+\infty}\frac{e^{-t^2}}{z-t}dt = e^{-z^2}\mathrm{erfc}(-iz), \tag{16}$$

and "erfc" in Eq. (16) is the Gauss error function, [95]–[96]. In the above expressions

$$Z_\pm = \sqrt{X+Y}\pm\sqrt{Y}, \tag{17}$$

$$X = \frac{-i(\nu_0-\nu)+\tilde{C}_0}{\tilde{C}_2}, Y = \left(\frac{\nu_0\nu_{a0}}{2c\tilde{C}_2}\right)^2, \tag{18}$$

$$\tilde{C}_0 = (1-\eta)\left(C_0-\frac{3C_2}{2}\right)+\nu_{\rm vc}, \tag{19}$$

and

$$\tilde{C}_2 = (1-\eta)C_2, \tag{20}$$

where $C_n = \Gamma_n + i\Delta_n$ $(n = 0, 2)$. To illustrate the quality of the analysis, Fig. 8 shows examples of the lineshape fits from which the line intensities have been determined.

For comparison, the results of the line shape fits for the $R(7, A_2)$ transition of all five isotopologues are shown. The value $\tau/(P \cdot L)$ (in units of $\mathrm{cm}^{-1}\mathrm{atm}^{-1}$) in Fig. 8 is given vs wavenumber ν and

$$\tau(\nu) = S^N_{\nu_0} \cdot F^{HT}(\nu - \nu_0) \cdot N \cdot L; \tag{21}$$

L is the optical path length; $F^{HT}(\nu - \nu_0)$ is the Hartmann–Tran profile function; and $S_{\nu_0} = (S^N_{\nu_0} \cdot N)$ is the individual line intensity which is determined in accordance with the formula, Eq. (5). The values which are necessary for the calculations have been taken in accordance with the discussion in Section 5. In this case, it was taken into account that, as the analysis showed, the studied sample contained also about 0.001% of CO_2, 0.17% of N_2O and 0.49% of H_2O.

At the second step of the analysis, the 556 experimental line intensities of the $^{74}GeH_4$ species mentioned above were used in the weighted fit of the effective dipole moment parameters (see Eq. (11)) and seven effective dipole moment parameters were obtained (parameters obtained from the fit are shown in column 7 of Table 6 together with their 1σ statistical confidence intervals which are given in parenthesis). These seven parameters, obtained from the fit, reproduce the 556 initial experimental line strengths of $^{74}GeH_4$ used in the analysis with the $d_{rms} = 3.42$ % (for more details see statistical information in the bottom part of Table 5). The d_{rms} value was determined in accordance with the formula

$$\left\{ \frac{1}{n} \sum_i \left(100 \times \frac{S^{N^{exp.}}_{\nu_i} - S^{N^{calc.}}_{\nu_i}}{S^{N^{exp.}}_{\nu_i}} \right)^2 \right\}^{1/2} \equiv \left\{ \frac{1}{n} \sum_i \delta_i^2 \right\}^{1/2}, \tag{22}$$

where n is the number of individual line strengths used in the fit.

Columns 4 and 5 of the Supplementary data 2 show experimental values of line strengths (in $\mathrm{cm}^{-2}\cdot\mathrm{atm}^{-1}$) and values δ_i (in per cent) of differences between the experimental line strengths and line strengths calculated with the parameters from column 7 of Table 6. For the convenience of the reader, a small part of the Supplementary data 2 is shown in Table 5. To illustrate the quality of the result, Fig. 9b

presents the fit residuals for line intensities as a function of the quantum number J (also see simulation of the spectra in the corresponding tracks of Figs. 1–6).

As the last step, the weighted fit of the effective dipole moment parameters of the four other isotopologues was made. In this case, the biggest part of the parameters of the $^{70}GeH_4$, $^{72}GeH_4$, $^{73}GeH_4$ and $^{76}GeH_4$ isotopologues was constrained to the values of corresponding parameters of the $^{74}GeH_4$ and was not varied in the fit procedure. Values of the $P^{(00A_1)}_{(0000,A_1)(0002,F_2)}$ parameters of the $^{73}GeH_4$ and $^{76}GeH_4$ isotopologues have been estimated from interpolation/extrapolation of the values of the $P^{(00A_1)}_{(0000,A_1)(0002,F_2)}$ parameters for the three other isotopologues. These two values also were not varied in the fit. The obtained values of fitted parameters are shown in columns 4, 5, 6 and 8 of Table 6. One can see a good correlation between values of different isotopologues. The 2, 2, 1 and 1 parameters obtained from the fit reproduce experimental strengths of 382, 511, 116 and 132 lines of $^{70}GeH_4$, $^{72}GeH_4$, $^{73}GeH_4$ and $^{76}GeH_4$ with the d_{rms} equal to 3.46, 3.49, 3.34 and 3.36 per cent, respectively. As for the $^{74}GeH_4$ molecule, the results of the line strengths calculation, as well as δ_i differences for the $^{70}GeH_4$, $^{72}GeH_4$, $^{73}GeH_4$ and $^{76}GeH_4$ species are shown in columns 4 and 5 of the Supplementary data 2. As a confirmation of the correctness of the results, see also Figs. 9a, 9c, 9d and 9e where the fit residuals for line intensities as functions of the quantum number J are presented, and the bottom tracks of Figs. 1 – 6.

7 Line shape analysis of the $2\nu_2/\nu_2+\nu_4/2\nu_4$ pentad bending triad of germane

For the line width analysis (full width at half maximum, FWHM), we exploited six spectra, IIa–IIf recorded at different pressures from 20 hPa up to 150 hPa (see Table 1 for details). Lines of the $\nu_2 + \nu_4(F_2)$ and $\nu_2 + \nu_4(F_1)$ sub–bands of the $\nu_2 + \nu_4$ band of all five isotopologues were analysed using a multi–spectrum fit with the Hartmann–Tran profile (see Fig. 10 where the same lines as in Fig. 8 are shown) in

accordance with the formula

$$\gamma = \gamma_{self} \times P \tag{23}$$

for the self–broadening $\gamma_{self}-$coefficient and

$$\delta_{\nu_0} = \delta_{self} \times P \tag{24}$$

for the shift $\delta_{self}-$coefficients. The obtained values of the $\gamma_{self}-$coefficients (for 993 lines) and $\delta_{self}-$coefficients (for 676 lines) are shown in columns 6 and 7 of the Supplementary data 2. For illustration of the quality of the performed analysis, the upper part of Fig. 10 presents the pressure dependence of the half–width for the same $R(7, A_2)$ transition of the $\nu_2 + \nu_4(F_2)$ band (spectra IIa–IIf) which are shown in Fig. 8. The bottom part of Fig. 10 illustrates the correctness of the determined self–broadening γ_{self} and shifts δ_{self} coefficients.

8 Conclusion

For the first time we present a comprehensive quantitative ro–vibrational study of line positions, strengths, widths and shifts in the high–resolution spectra of the pentad bending triad of all five stable germane isotopologues. We performed the joint ro–vibrational analysis of 16422 line positions in 35 "cold" and 23 "hot" bands of the $^{70}GeH_4$, $^{72}GeH_4$, $^{73}GeH_4$, $^{74}GeH_4$, $^{76}GeH_4$ isotopologues and obtained a set of 129 effective spectroscopic parameters (upper vibrational energies, rotational, centrifugal distortion, tetrahedral and resonance interaction parameters) from the weighted fit which reproduce the initial 16422 experimental line positions with the $d_{\rm rms} = 3.26 \times 10^{-4}$ cm^{-1}. Line strengths of 1697 individual ro–vibrational lines belonging to the thirty five different bands of all five isotopologues were obtained from the fit of their experimental line shapes with the Hartmann–Tran profile. A set of 13 effective dipole moment parameters obtained from the weighted fit allows one to reproduce 1697 experimental line strength with the $d_{\rm rms} = 3.4\%$. Self–broadening and self–shifts coefficients are obtained for the same 1697 lines of the pentad bending

triad of germane. The present data will be soon included in the VAMDC/GeCaSDa database [33].

9 Acknowledgments

The research was funded by the Tomsk Polytechnic University Competitiveness Enhancement Program (project VIU189/2020), and by the Deutsche Forschungsgemeinschaft (grants BA 2176/4-1, BA 2176/4-2, and BA 2176/5- 1).

10 Figure captions

Fig. 1. Experimental survey spectrum I of germane in the region of the first dyad (upper trace 1a). Experimental conditions: absorption path length is 24 m; room temperature $(23.6 \pm 0.1)^o$C; number of scans is 1400; sample pressure is 250 Pa. Traces (1c)–(1g) show the simulated spectra of separate germane isotopologues; trace (1b) is the global simulated spectrum as a sum of the simulated (1c)–(1g) spectra. Lines belonging to the $\nu_2 + \nu_4$, $2\nu_4$ and $2\nu_2$ bands are marked by the black, orange and red color.

Fig. 2. Experimental survey spectrum IIa of germane in the region of the first dyad $\nu_2 + \nu_4$ band (upper trace). Experimental conditions: absorption path length is 0.23 m; room temperature $(23.8 \pm 0.3)^o$C; number of scans is 400; sample pressure is 20 hPa. The lower trace shows the corresponding simulated spectrum.

Fig. 3. Small part of the high resolution experimental spectrum IIa of germane in the region of the $\nu_2 + \nu_4$ band (upper trace). The lower trace shows the corresponding simulated spectrum. The cluster $P(9, \Gamma)$ ($\Gamma = A_2, F_2, F_1$ and A_1) of the $\nu_2 + \nu_4(F_2)$ sub–band of all five ^{M}GeH$_4$ isotopologues is marked.

Fig. 4. Small part of the high resolution experimental spectrum IIa of germane in the region of the $\nu_2 + \nu_4$ band (upper trace). The lower trace shows the corresponding simulated spectrum. The cluster $R(8, \Gamma)$ ($\Gamma = E, F_1$ and A_1) of the $\nu_2 + \nu_4(F_2)$ sub–band of all five ^{M}GeH$_4$ isotopologues is marked.

Fig. 5. Small part of the high resolution experimental spectrum I of germane in the region of the $2\nu_4$ band (upper trace). The lower traces (5c)–(5g) show the corresponding simulated spectra for the individual isotopologues. The cluster $P(12, \Gamma)$ ($\Gamma = E, F_1$ and A_1) of the $2\nu_4(F_2)$ sub–band of all five ^{M}GeH$_4$ isotopologues is marked. Trace (5b) is the global simulated spectrum as the sum of the simulated

(5c)–(5g) spectra .

Fig. 6. Small part of the high resolution experimental spectrum I of germane in the region of the $2\nu_2$ band (upper trace). Lower traces (5c)–(5g) show the corresponding simulated spectra for the individual isotopologues. The clusters $Q(9,\Gamma)$ ($\Gamma = F_2, F_1$ and A_1) and $Q(10,\Gamma)$ ($\Gamma = A_2, F_2$ and E) of the $2\nu_2(E)$ sub–band of all five $^{M}GeH_4$ isotopologues is marked. Trace (5b) is the global simulated spectrum as the sum of simulated (5c)–(5g) spectra .

Fig. 7. Observed minus calculated line positions and fit statistics for "cold" bands studied in the present paper of the $^{74}GeH_4$, $^{72}GeH_4$ and $^{70}GeH_4$ species.

Fig. 8. Experimental line shape of the $R(7, A_2)$ transition of the $\nu_2 + \nu_4(F_2)$ band for five different isotopologues of germane (for experimental conditions, see Section 2 and Table 1). The fit of the experimental line shapes was made with the Hartmann–Tran profile of individual lines. The solid and dashed lines correspond to the experimental and calculated value of $\tau(\tilde{\nu})$. The bottom part of the figures shows the (exp.−calc.) residuals.

Fig. 9. Observed minus calculated line intensities (in per cent) including fit statistics for the $2\nu_2$, $\nu_2 + \nu_4$ and $2\nu_4$ bands of the five stable isotopologues of germane.

Fig. 10. Upper part: Examples of FTIR line spectra IIa–IIf recorded at different pressures for the $R(7, A_2)$ transition of the $\nu_2+\nu_4(F_2)$ band for five different isotopologues of germane (for experimental conditions, see Section 2 and Table 1). Bottom part: measured self–broadening and maximum line–shift coefficients at room temperature vs pressure.

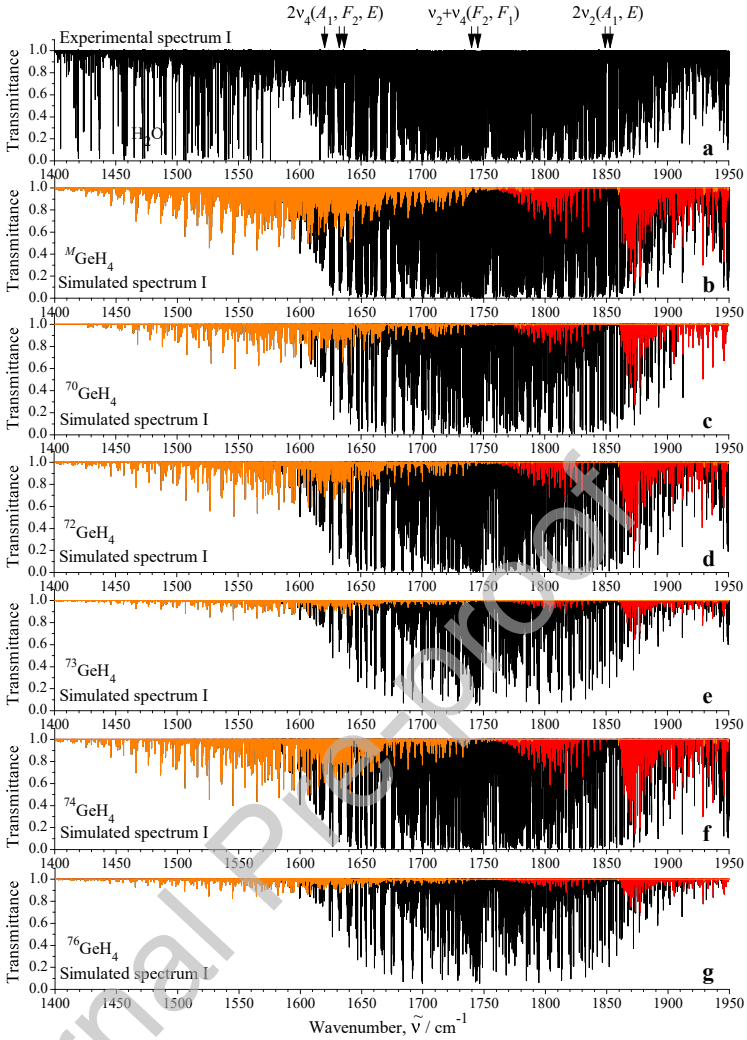

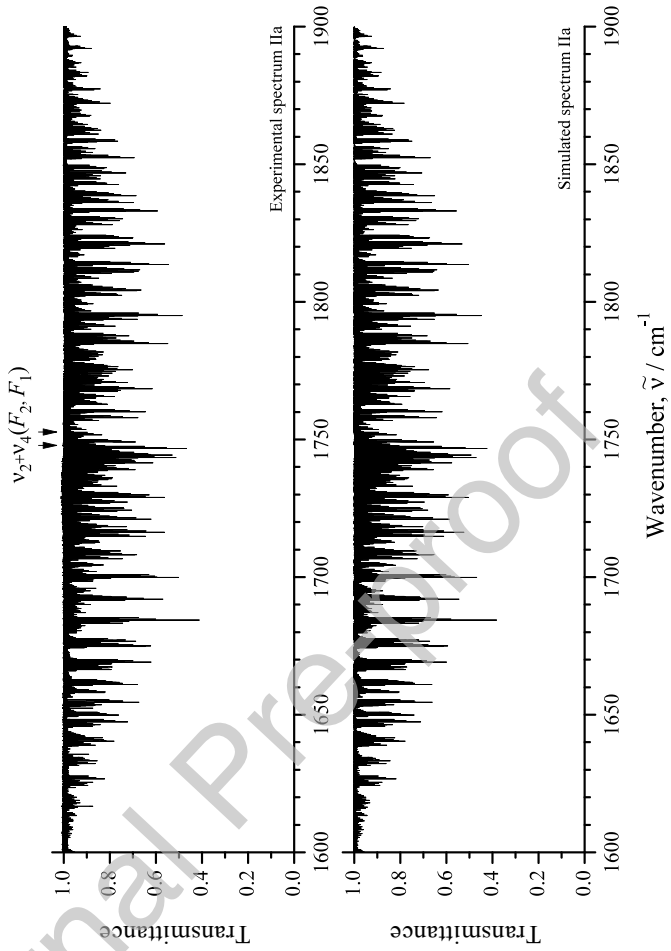

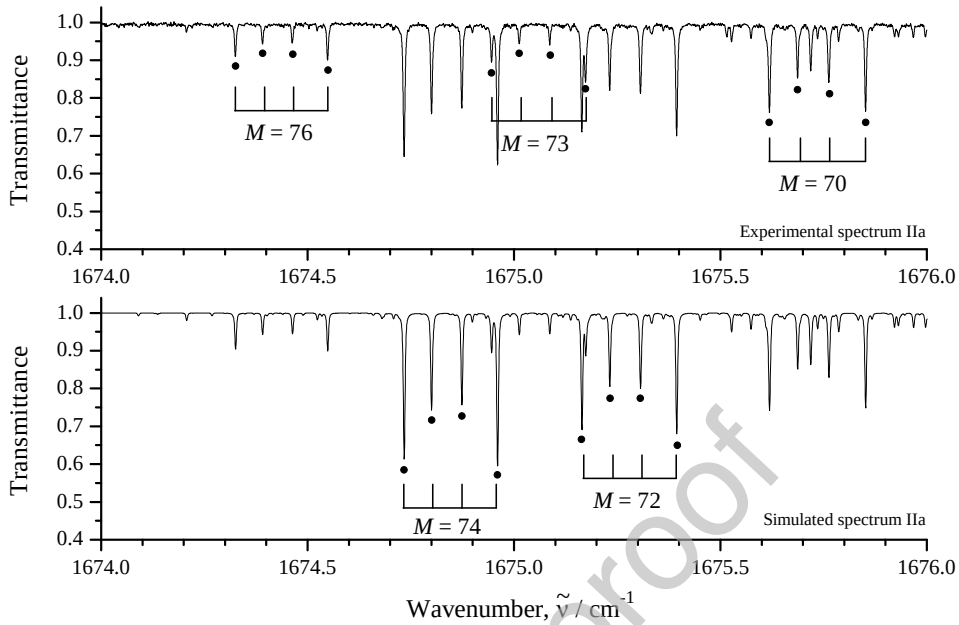

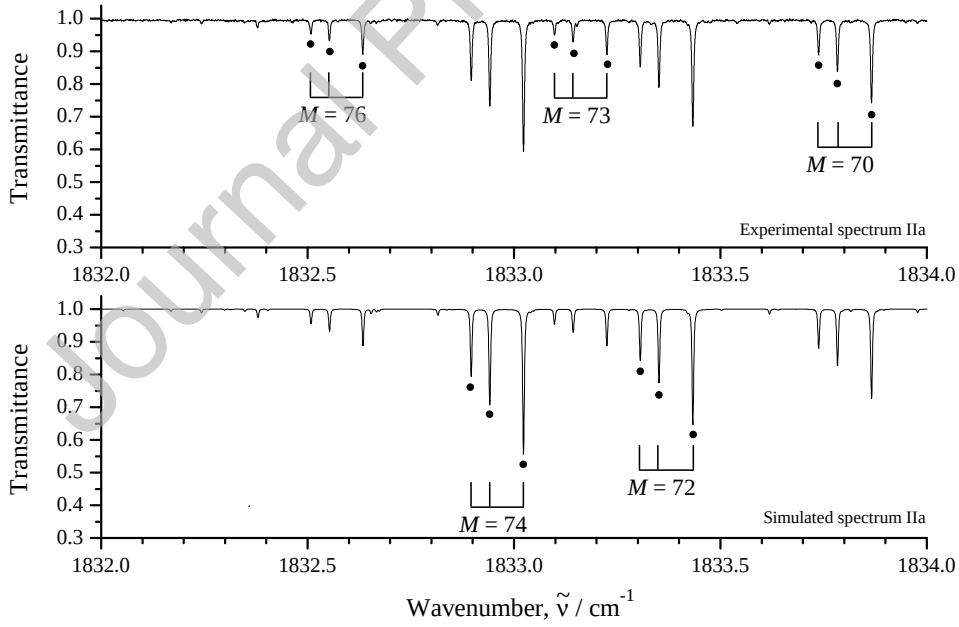

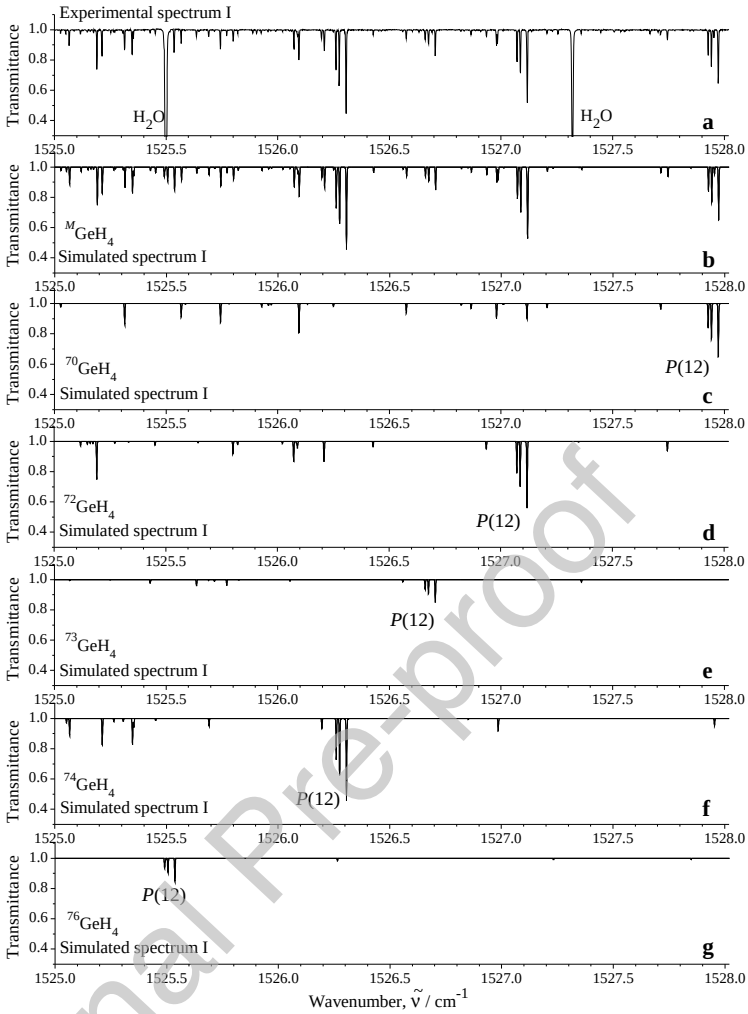

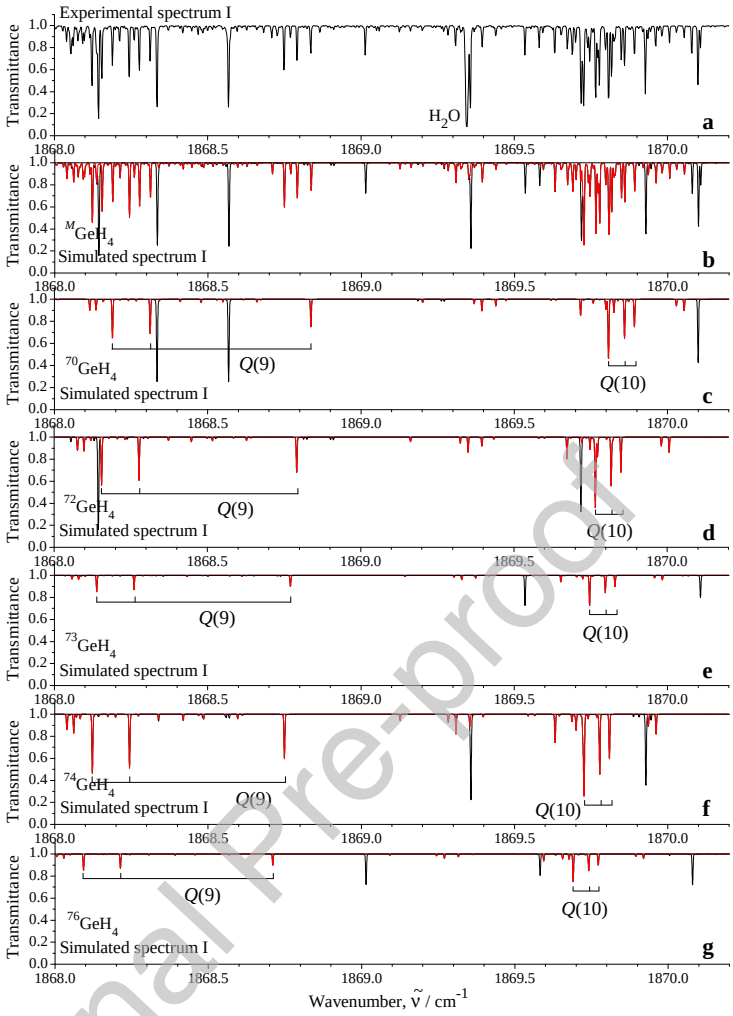

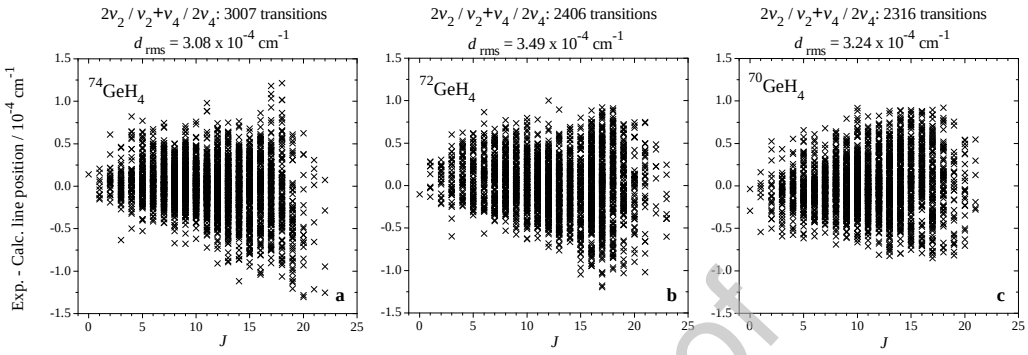

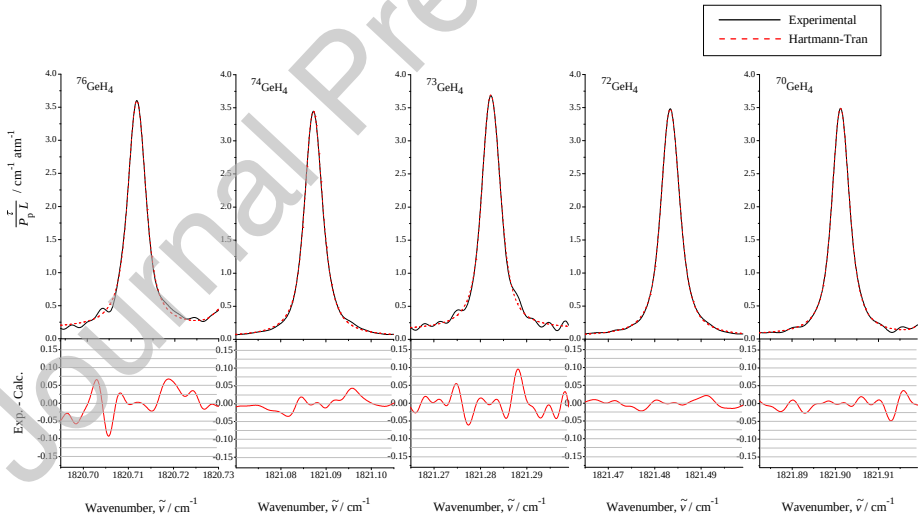

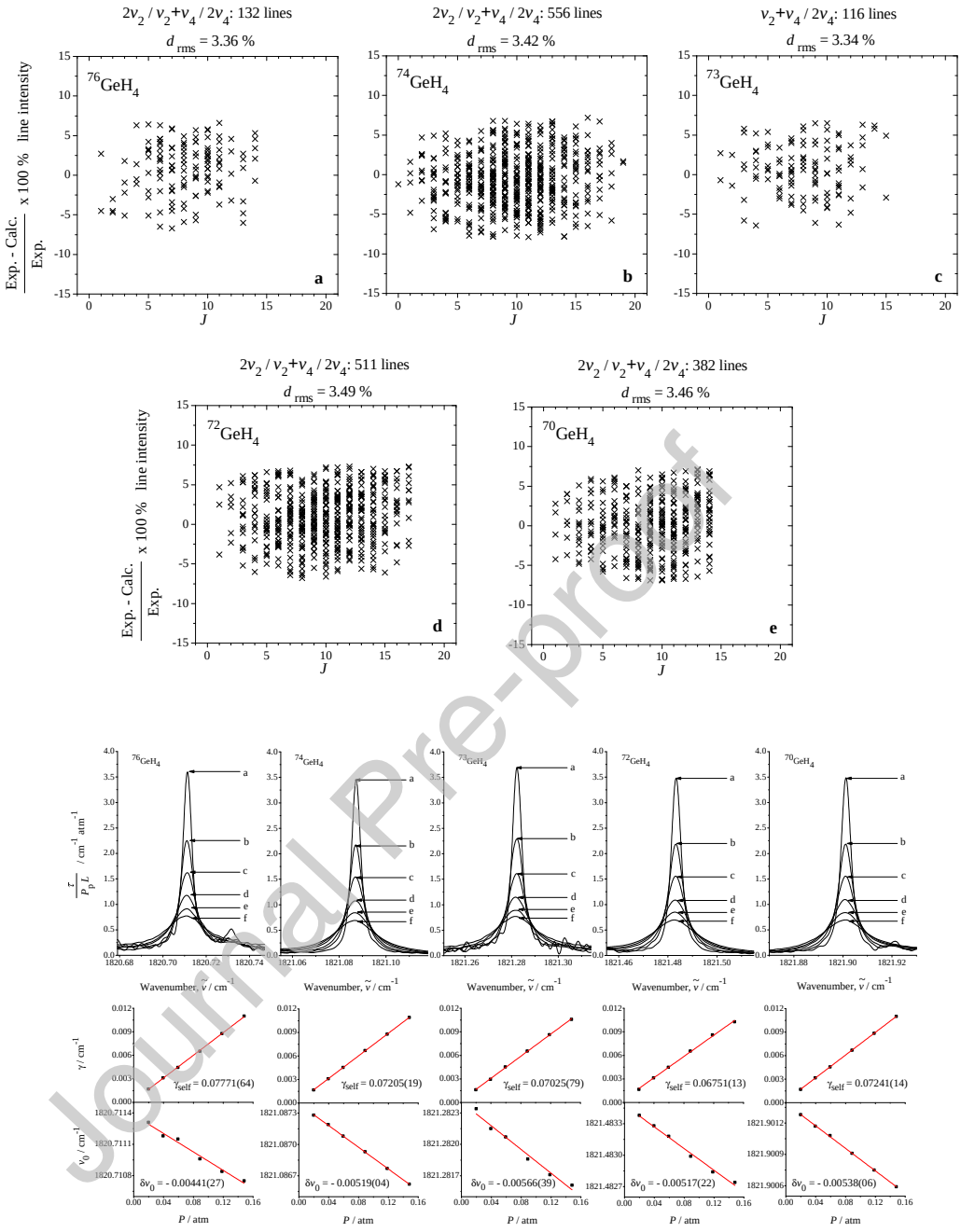

Table 1. Experimental setup of the infrared spectra of $^{M}GeH_4$ (M=70, 72, 73, 74, 76).

Spectrum	Region /cm^{-1}	Resolution /cm^{-1}	No. of scans	Source	Detector	Beam-splitter	Opt. path-length/m	Temp. /°C	Pressure /Pa	Calibr. gas
I	600 - 4800	0.003	1400	Globar	MCT313	KBr	24	23.6 ± 0.1	250	H_2O, N_2O
IIa	1400 - 2700	0.003	400	Globar	MCT313	KBr	0.23	23.8 ± 0.3	2000	H_2O
IIb	1400 - 2700	0.003	300	Globar	MCT313	KBr	0.23	23.7 ± 0.3	4000	H_2O
IIc	1400 - 2700	0.003	520	Globar	MCT313	KBr	0.23	23.6 ± 0.3	6000	H_2O
IId	1400 - 2700	0.003	600	Globar	MCT313	KBr	0.23	23.5 ± 0.7	9000	H_2O
IIe	1400 - 2700	0.003	680	Globar	MCT313	KBr	0.23	23.4 ± 0.7	12000	H_2O
IIf	1400 - 2700	0.003	600	Globar	MCT313	KBr	0.23	23.5 ± 0.7	15000	H_2O

Table 2. Statistical information for the $2\nu_2(A_1, E)$, $\nu_2 + \nu_4(F_1, F_2)$ and $2\nu_4(A_1, E, F_2)$ bands of $^{M}GeH_4$ (M = 70, 72, 73, 74, 76).

Band	Energy[a]/cm^{-1}	J^{max}	N_{tr}[b]	N_l[c]	m_1[d]	m_2[d]	m_3[d]	
1	2	3	4	5	6	7	8	9
			$^{76}GeH_4$					
$2\nu_4(A_1) - \nu_4(F_2)$	1627.4950	11	76	29	78.9	11.9	9.2	[1]
$2\nu_4(F_2) - \nu_4(F_2)$		15	206		70.4	21.4	8.2	[1]
$2\nu_4(F_2)$	1639.2570	15	100	189	54.6	24.8	20.6	[1]
$2\nu_4(E) - \nu_4(F_2)$		15	52		78.8	13.5	7.7	[1]
$2\nu_2(E)$	1642.1422	13	28	43	35.7	28.6	35.7	[1]
$\nu_2 + \nu_4(F_2) - \nu_4(F_2)$		16	119		56.2	28.1	15.7	[1]
$\nu_2 + \nu_4(F_2) - \nu_2(E)$		15	236		51.4	31.3	17.3	[1]
$\nu_2 + \nu_4(F_2)$	1748.3962	19	793	401	59.9	26.5	13.6	[1]
$\nu_2 + \nu_4(F_1) - \nu_4(F_2)$		15	45		59.2	22.5	18.3	[1]
$\nu_2 + \nu_4(F_1) - \nu_2(E)$		15	179		59.6	30.1	10.3	[1]
$\nu_2 + \nu_4(F_1)$	1752.5031	18	699	289	71.5	19.9	8.6	[1]
$2\nu_2(A_1)$	1857.2721	18	131	64	73.1	15.9	11.0	[1]
$2\nu_2(E) - \nu_2(E)$		17	81		55.6	32.1	12.3	[1]
$2\nu_2(E)$	1860.6673	19	503	257	80.8	12.7	6.5	[1]
Total N_{tr} (cold bands)			2254					[1]
Total N_{tr} (hot bands)			994					[1]
Total N_l				1272				[1]
d_{rms} (cold bands)	2.64 × 10^{-4}cm^{-1}							[1]
d_{rms} (hot bands)	2.91 × 10^{-4}cm^{-1}							[1]
			$^{74}GeH_4$					
$2\nu_4(A_1)$	1628.2541	11	17	7	53.0	47.0	0.0	tw
$2\nu_4(F_2)$	1640.0175	17	280	161	66.1	25.7	8.2	tw
$2\nu_2(E)$	1642.9085	17	82	48	75.6	14.6	9.8	tw
$\nu_2 + \nu_4(F_2) - \nu_2(E)$		12	50					[1]
$\nu_2 + \nu_4(F_2)$	1748.7773	15	159	156	71.3	21.5	7.2	[1]
$\nu_2 + \nu_4(F_2)$	1748.7768	22	1171	455	60.9	23.7	15.4	tw
$\nu_2 + \nu_4(F_1) - \nu_2(E)$		11	69					[1]
$\nu_2 + \nu_4(F_1)$	1752.8865	13	150	129	58.8	28.1	13.1	[1]
$\nu_2 + \nu_4(F_1)$	1752.8864	22	1018	546	75.5	16.8	7.7	tw
$2\nu_2(A_1)$	1857.2650	16	77	42	42.9	28.6	28.5	tw
$2\nu_2(E)$	1860.6595	21	362	200	43.7	28.5	27.8	tw
Total N_{tr} (cold bands)			3007					tw
Total N_{tr} (hot bands)			99					[1]
Total N_l				1459				tw
d_{rms} (cold bands)	3.08 × 10^{-4}cm^{-1}							tw
d_{rms} (hot bands)	2.9 × 10^{-4}cm^{-1}							[1]
			$^{73}GeH_4$					
$2\nu_4(A_1) - \nu_4(F_2)$	1628.6480	19	268	128	66.3	18.8	14.9	[2]
$2\nu_4(F_2) - \nu_4(F_2)$	1640.4120	22	665	445	70.0	19.7	10.3	[2]
$2\nu_4(E) - \nu_4(F_2)$	1643.3059	19	171	105	72.8	15.2	12.0	[2]
$\nu_2 + \nu_4(F_2) - \nu_2(E)$		19	399		63.8	25.8	10.4	[2]
$\nu_2 + \nu_4(F_2) - \nu_4(F_2)$		16	133		57.3	29.8	12.9	[2]
$\nu_2 + \nu_4(F_2)$	1748.9748	18	465	419	74.2	16.2	9.6	[2]
$\nu_2 + \nu_4(F_1) - \nu_2(E)$		19	394		67.0	22.4	10.6	[2]
$\nu_2 + \nu_4(F_1) - \nu_4(F_2)$		17	69		65.2	26.1	8.7	[2]
$\nu_2 + \nu_4(F_1)$	1753.0849	16	294	337	70.1	25.2	4.7	[2]
$2\nu_2(A_1) - \nu_2(E)$	1857.2607	14	8	7	62.5	37.5	0.0	[2]
$2\nu_2(E) - \nu_2(E)$		19	12		41.7	41.7	16.6	[2]
$2\nu_2(E)$	1860.6552	14	114	94	52.7	28.1	19.2	[2]
Total N_{tr} (cold bands)			873					[2]
Total N_{tr} (hot bands)			2119					[2]
Total N_l				1535				[2]
d_{rms} (cold bands)	2.55 × 10^{-4}cm^{-1}							[2]
d_{rms} (hot bands)	3.00 × 10^{-4}cm^{-1}							[2]
			$^{72}GeH_4$					
$2\nu_4(A_1) - \nu_4(F_2)$		20	299		67.1	22.4	10.5	[3]
$2\nu_4(A_1)$	1629.0544	20	131	153	47.4	31.3	21.3	tw
$2\nu_4(F_2) - \nu_4(F_2)$		20	692		58.2	24.5	17.3	[3]
$2\nu_4(F_2)$	1640.8186	22	578	507	53.4	26.8	17.8	tw
$2\nu_4(E) - \nu_4(F_2)$		20	213		59.9	21.3	18.8	[3]
$2\nu_4(E)$	1643.7157	21	138	144	43.1	31.9	25.0	tw
$\nu_2 + \nu_4(F_2) - \nu_2(E)$		19	400		65.3	23.5	11.2	[3]
$\nu_2 + \nu_4(F_2) - \nu_4(F_2)$		17	146		65.8	22.6	11.6	[3]
$\nu_2 + \nu_4(F_2)$	1749.1787	16	364	385	73.6	20.6	5.8	[3]
$\nu_2 + \nu_4(F_2)$	1749.1788	23	793	515	58.9	23.5	17.6	tw
$\nu_2 + \nu_4(F_1) - \nu_2(E)$		19	406		64.9	22.8	12.3	[3]
$\nu_2 + \nu_4(F_1) - \nu_4(F_2)$		17	82		63.4	23.2	13.4	[3]
$\nu_2 + \nu_4(F_1)$	1753.2897	16	183	337	78.7	16.4	4.9	[3]
$\nu_2 + \nu_4(F_1)$	1753.2898	23	396	412	52.3	27.3	20.4	tw
$2\nu_2(A_1) - \nu_2(E)$		14	5	4	40.0	60.0	0.0	[3]
$2\nu_2(A_1)$	1857.2576	17	67	45	37.4	37.4	25.2	tw
$2\nu_2(E) - \nu_2(E)$		17	106		46.2	32.7	21.1	[3]
$2\nu_2(E)$	1860.6516	20	393	254	41.7	28.5	29.8	tw
Total N_{tr} (cold bands)			2406					tw
Total N_{tr} (hot bands)			2351					[3]
Total N_l				2030				tw
d_{rms} (cold bands)	3.49 × 10^{-4}cm^{-1}							tw
d_{rms} (hot bands)	3.11 × 10^{-4}cm^{-1}							[3]
			$^{70}GeH_4$					
$2\nu_4(A_1)$	1629.8994	16	35	22	57.2	25.7	17.1	tw
$2\nu_4(F_2)$	1641.6643	18	409	291	50.4	29.6	20.0	tw
$2\nu_4(E)$	1644.5675	16	115	74	55.7	33.1	11.2	tw
$\nu_2 + \nu_4(F_2)$	1749.6024	21	839	418	53.8	23.9	22.3	tw
$\nu_2 + \nu_4(F_1)$	1753.7155	21	794	329	67.4	21.7	10.9	tw
$2\nu_2(A_1)$	1857.2505	13	4	3	25.0	50.0	25.0	tw
$2\nu_2(E)$	1860.6437	20	120	91	37.5	28.4	65.9	tw
Total N_{tr} (cold bands)			2316					tw
Total N_l				1228				tw
d_{rms} (cold bands)	3.24 × 10^{-4}cm^{-1}							tw

[a] Value of the upper vibrational energy.
[b] N_{tr} is the number of assigned transitions.
[c] N_l is the number of obtained upper-state energies.
[d] Here $m_i = n_i/N_{tr} \times 100$ % (i = 1, 2, 3); n_1, n_2, and n_3 are the numbers of transitions for which the differences $\delta = \nu^{\mathrm{exp}} - \nu^{\mathrm{calc}}$ satisfy the conditions $\delta \leq 2 \times 10^{-4}$ cm^{-1}, 2×10^{-4} cm^{-1} $< \delta \leq 4 \times 10^{-4}$ cm^{-1}, and $\delta > 4 \times 10^{-4}$ cm^{-1}.

a e 3 ec r sc ic arame ers $\Omega(K\ \Gamma)$ $_{v\ v'\ \gamma'}$ e se in erac in vi ra i na s a es (0002)(0101) (0200) in e 4 (in cm $^{1})^{a)}$

(v,γ)	(v',γ')	$\Omega(K,n\Gamma)$	^{70} e $_{4}$	^{72} e $_{4}$	^{73} e $_{4}$	^{74} e $_{4}$	^{7} e $_{4}$
1	2	3	4	5	6	7	
(0200, A_1)	(0200, A_1)	0(0, A_1)	2 6 369	2 6 369	2 6 369	2 6 369	2 6 369
	(0200, A_1)	2(0, A_1)10^3	0 4716	0 4716	0 4716	0 4716	0 4716
(0200, A_1)	(0200,)	2(2,)10^3	0 256300(53)	0 256050(67)	0 255925(4)	0 255 00(69)	0 255550(52)
(0200,)	(0200,)	0(0, A_1)	0 409419(71)	0 409 73(4)	0 410100(69)	0 40 000( )	0 4107 1(62)
	(0200,)	2(2,)10^3	0 3393	0 3393	0 3393	0 3393	0 3393
	(0200,)	3(3, A_2)10	0 26045	0 26045	0 26045	0 26045	0 26045
(0200, A_1)	(0101, F_2)	2(2, F_2)10^3	0 11	0 11	0 11	0 11	0 11
(0200,)	(0101, F_1)	1(1, F_1)	0 02657 5( )	0 026651 3(1)	0 0267024( )	0 0267437(42)	0 026 263(52)
	(0101, F_1)	2(2, F_2)10^3	0 21017	0 21017	0 21017	0 21017	0 21017
	(0101, F_1)	3(3, F_2)10	0 4234	0 4234	0 4234	0 4234	0 4234
(0200,)	(0101, F_2)	1(1, F_1)	0 03145 2(32)	0 0316 10(10)	0 0317159(24)	0 03191 0(12)	0 0319736(22)
	(0101, F_2)	3(1, F_1)10	0 4543	0 4543	0 4543	0 4543	0 4543
(0200, A_1)	(0002, A_1)	0(0, A_1)	5 46 35( )	5 46143(16)	5 45797( )	5 4561 (19)	5 45261(14)
	(0002, A_1)	2(0, A_1)10^3	0 49 91( )	0 51523(50)	0 52339( )	0 52959(63)	0 5419 (70)
(0200,)	(0002,)	0(0, A_1)	0 196 59(35)	0 1 3966(51)	0 17752(11)	0 170639(39)	0 15 17(14)
	(0002,)	2(2,)10^3	0 45655( )	0 4627 (41)	0 46590( )	0 46902(35)	0 47525(3)
(0200,)	(0002, F_2)	1(1, F_1)	0 2300 46(47)	0 2305662(91)	0 230 070(49)	0 2310334(96)	0 2314435(44)
	(0002, F_2)	3(1, F_1)10	0 3016	0 3016	0 3016	0 3016	0 3016
(0101, F_1)	(0101, F_1)	0(0, A_1)	2 269 322(64)	2 2677959(6)	2 266777 (5)	2 2652072(64)	2 2635159(64)
	(0101, F_1)	1(1, F_1)	0 0510521	0 0510521	0 0510521	0 0510521	0 0510521
	(0101, F_1)	2(0, A_1)10	0 509	0 509	0 509	0 509	0 509
	(0101, F_1)	2(2, F_2)10^3	0 7694	0 7694	0 7694	0 7694	0 7694
(0101, F_1)	(0101, F_2)	1(1, F_1)	0 0565 910(33)	0 056470 2(57)	0 0564319(20)	0 05636944(60)	0 0562747(25)
	(0101, F_2)	2(2,)10^4	0 7774	0 7774	0 7774	0 7774	0 7774
	(0101, F_2)	2(2, F_2)10^3	0 79071	0 79071	0 79071	0 79071	0 79071
	(0101, F_2)	3(1, F_1)10	0 5 1 1	0 5 1 1	0 5 1 1	0 5 1 1	0 5 1 1
(0101, F_2)	(0101, F_2)	0(0, A_1)	2 015121 (63)	2 0143 17(66)	2 0140117(2)	2 014759 (52)	2 013554(10)
	(0101, F_2)	1(1, F_1)	0 05499 2( )	0 054 642(13)	0 0547972( )	0 0547456(67)	0 0546425(9)
	(0101, F_2)	2(0, A_1)10^3	0 37 9 ( )	0 37 744(61)	0 37 622( )	0 37 500(56)	0 37 256(75)
	(0101, F_2)	2(2,)10^3	0 3357	0 3357	0 3357	0 3357	0 3357
	(0101, F_2)	2(2, F_2)10^3	0 515	0 515	0 515	0 515	0 515
	(0101, F_2)	3(1, F_1)10^4	0 1 456	0 1 456	0 1 456	0 1 456	0 1 456
	(0101, F_2)	3(3, F_1)10^4	0 14931	0 14931	0 14931	0 14931	0 14931
(0101, F_1)	(0002, A_1)	1(1, F_1)	0 0647354(46)	0 06520650(75)	0 0654537(49)	0 06561 (55)	0 0659491(3)
(0101, F_1)	(0002,)	1(1, F_1)10^3	0 2 99	0 2 99	0 2 99	0 2 99	0 2 99
(0101, F_1)	(0002, F_2)	1(1, F_1)10^2	0 14314(40)	0 12377(36)	0 11409(37)	0 104 2(40)	0 0 504(53)
	(0002, F_2)	2(2,)10^3	0 15012( )	0 15230(23)	0 15344( )	0 15455(15)	0 15676(17)
	(0002, F_2)	2(2, F_2)10	0 1592	0 1592	0 1592	0 1592	0 1592
	(0002, F_2)	3(1, F_2)10	0 294	0 294	0 294	0 294	0 294
	(0002, F_2)	3(3, A_2)10	0 3359	0 3359	0 3359	0 3359	0 3359
	(0002, F_2)	3(3, F_1)10	0 9951	0 9951	0 9951	0 9951	0 9951
	(0002, F_2)	3(3, F_2)10	0 692	0 692	0 692	0 692	0 692
(0101, F_2)	(0002, A_1)	2(2, F_2)10^3	0 3 79	0 3 79	0 3 79	0 3 79	0 3 79
	(0002, A_1)	3(3, F_2)10	0 1653 ( )	0 19259(49)	0 20619( )	0 21979(70)	0 2479(12)
(0101, F_2)	(0002,)	3(1, F_1)10^4	0 14660( )	0 14509(19)	0 14434( )	0 14359(11)	0 1420 (16)
(0101, F_2)	(0002, F_2)	0(0, A_1)	4 3042400(1)	4 3029156(92)	4 30197 (66)	4 3013164(97)	4 299716(6)
	(0002, F_2)	1(1, F_1)	0 0255963(1)	0 02563302(2)	0 0257512(43)	0 0257927(7)	0 025 75 (55)
	(0002, F_2)	2(0, A_1)10^3	0 63352	0 63352	0 63352	0 63352	0 63352
	(0002, F_2)	2(2,)10^4	0 2 56	0 2 56	0 2 56	0 2 56	0 2 56
	(0002, F_2)	3(1, F_1)10	0 14470( )	0 139 7(71)	0 13742( )	0 13499(56)	0 13014(5)
	(0002, F_2)	3(3, F_2)10^4	0 14725	0 14725	0 14725	0 14725	0 14725
(0002, A_1)	(0002, A_1)	0(0, A_1)	13 057692(23)	13 04 400(27)	13 043753(11)	13 039565(19)	13 029 25(13)
	(0002, A_1)	2(0, A_1)10^4	0 1675	0 1675	0 1675	0 1675	0 1675
(0002, A_1)	(0002,)	2(2,)10^3	0 20973 ( )	0 212909 (23)	0 216019( )	0 21 11(60)	0 22230(16)
(0002, A_1)	(0002, F_2)	2(2, F_2)10^3	0 295192( )	0 29927 (3)	0 301321( )	0 303364(65)	0 30745(2)
	(0002, F_2)	3(3, F_2)10^4	0 09 70 ( )	0 100399(11)	0 10124 ( )	0 103529(77)	0 10 09(30)
(0002,)	(0002,)	0(0, A_1)	1 479011( )	1 4 23090(12)	1 4 395 1( )	1 4 4975(9)	1 4 355(16)
	(0002,)	2(2,)10^3	0 522400( )	0 5216 0 (49)	0 521325( )	0 520967(3)	0 52025(15)
	(0002,)	3(3, A_2)10^4	0 10591	0 10591	0 10591	0 10591	0 10591
(0002,)	(0002, F_2)	1(1, F_1)	0 03036044( )	0 03030544(45)	0 03025272( )	0 030216 1(75)	0 0301450(13)
	(0002, F_2)	2(2, F_2)10^3	0 596369( )	0 59 0 (63)	0 600027( )	0 60013 (67)	0 60036(15)
	(0002, F_2)	3(1, F_1)10	0 353	0 353	0 353	0 353	0 353
	(0002, F_2)	3(3, F_1)10	0 196	0 196	0 196	0 196	0 196
	(0002, F_2)	3(3, F_2)10	0 5111	0 5111	0 5111	0 5111	0 5111
(0002, F_2)	(0002, F_2)	0(0, A_1)	1 2525012(6)	1 2437923(2)	1 2394022(75)	1 235 05(11)	1 227372(10)
	(0002, F_2)	1(1, F_1)	0 033173 ( )	0 0331210(41)	0 03310 5( )	0 0330 67(6)	0 0330432(94)
	(0002, F_2)	2(0, A_1)10^4	0 147	0 147	0 147	0 147	0 147
	(0002, F_2)	2(2,)10^3	0 119	0 119	0 119	0 119	0 119
	(0002, F_2)	2(2, F_2)10^3	0 59665(53)	0 5911 (6)	0 5 44(5)	0 5 570(76)	0 5 023(49)
	(0002, F_2)	3(1, F_1)10	0 3567	0 3567	0 3567	0 3567	0 3567
	(0002, F_2)	3(3, F_1)10	0 5775	0 5775	0 5775	0 5775	0 5775

$^{a)}$ a cs in aren eses a d lo s a is ica c n ence in erva s arame ers resen e i c n ence in erva s ere c ns raine e va es c rres n in arame ers e ^{7} e $_{4}$ ^{73} e $_{4}$ r ^{72} e $_{4}$ is es r m e s 1 2 r 3 arame ers ^{70} e $_{4}$ an ^{73} e $_{4}$ ic are mar e s ar ere aine r m in er a i n ex ra a i n e va es c rres n in arame ers e ree er s ecies an ere n varie in e

a e 4 ec r sc ic arame ers $\Omega(K\ \Gamma)$ $_{v\ v'\ ,}$ e r n an (0100) (0001) vi ra i na s a es e 4 (in cm ^{1})[a)]

(v,γ)	(v',γ')	$\Omega(K,n\Gamma)$	^{70} e 4	^{72} e 4	^{73} e 4	^{74} e 4	^{7} e 4
1	2	3	4	5	6	7	
(0000, A_1)	(0000, A_1)	2(0, A_1)	2 695 5536	2 695 5944	2 695 629	2 695 64734	2 695 70305
	(0000, A_1)	4(0, A_1)10^4	0 33416 2	0 33416 2	0 33416 2	0 33416 2	0 33416 2
	(0000, A_1)	4(4, A_1)10	0 1547079	0 1547079	0 1547079	0 1547079	0 1547079
	(0000, A_1)	6(0, A_1)10	0 11436	0 11436	0 11436	0 11436	0 11436
	(0000, A_1)	6(4, A_1)10^{10}	0 51075	0 51075	0 51075	0 51075	0 51075
	(0000, A_1)	6(6, A_1)10^{10}	0 1563	0 1563	0 1563	0 1563	0 1563
(0100,)	(0100,)	0(0, A_1)	929 901299	929 905235	929 9070022	929 9093056	929 9130275
	(0100,)	2(2,)10^1	0 107 392	0 107 392	0 107 7 1	0 107 7 1	0 107 743
	(0100,)	3(3, A_2)10^4	0 2265992	0 2265992	0 2261	0 2261	0 2261
	(0100,)	4(0, A_1)10	0 4052	0 4052	0 4052	0 4052	0 4052
	(0100,)	4(2,)10	0 31077	0 31077	0 31077	0 31077	0 31077
	(0100,)	4(4, A_1)10^7	0 134	0 134	0 134	0 134	0 134
	(0100,)	4(4,)10	0 125 3	0 125 3	0 125 3	0 125 3	0 125 3
(0100,)	(0001, F_2)	1(1, F_1)	4 51245 6	4 5091962	4 507623	4 506094	4 503062
	(0001, F_2)	2(2, F_2)	0 02127619	0 0212915 6	0 02129422	0 021300795	0 021316
	(0001, F_2)	3(1, F_1)10^3	0 1179753	0 1179753	0 1179267	0 1179267	0 1179267
	(0001, F_2)	3(3, F_2)10^4	0 136921	0 136921	0 13 096	0 13 096	0 13 096
	(0001, F_2)	4(2, F_2)10	0 212431	0 212431	0 2122	0 2122	0 2122
	(0001, F_2)	4(4, F_1)10	0 1 552	0 1 552	0 1 552	0 1 552	0 1 552
	(0001, F_2)	4(4, F_2)10	0 209 79	0 209 79	0 209 79	0 209 79	0 209 79
	(0001, F_2)	5(1, F_1)10	0 23013	0 23013	0 23013	0 23013	0 23013
	(0001, F_2)	5(3, F_1)10	0 13677	0 13677	0 13677	0 13677	0 13677
	(0001, F_2)	5(3, F_2)10	0 5 5	0 5 5	0 5 5	0 5 5	0 5 5
(0001, F_2)	(0001, F_2)	0(0, A_1)	21 5443402	21 1167767	20 9110 61	20 711 50	20 3270025
	(0001, F_2)	1(1, F_1)	6 3712225	6 37 46454	6 3 19626	6 3 534 5	6 391 6203
	(0001, F_2)	2(0, A_1)10^2	0 10 2241	0 1075775	0 1070517	0 10672 96	0 1060455
	(0001, F_2)	2(2,)10^2	0 152390	0 1509974	0 1504 33	0 149 614	0 14 49411
	(0001, F_2)	2(2, F_2)	0 01070173	0 010699349	0 01069594	0 0106 462	0 0106923
	(0001, F_2)	3(1, F_1)10^4	0 702161	0 7027 3	0 70411	0 7047 9	0 70545
	(0001, F_2)	3(3, F_1)10^4	0 4 0174	0 4 0174	0 479437	0 47902	0 47902
	(0001, F_2)	4(0, A_1)10	0 370472	0 370472	0 3653	0 3653	0 3653
	(0001, F_2)	4(2, F_2)10	0 3519	0 3519	0 3519	0 3519	0 3519
	(0001, F_2)	4(4, A_1)10^7	0 6407	0 6407	0 6407	0 6407	0 6407
	(0001, F_2)	5(1, F_1)10	0 25953	0 25953	0 25953	0 25953	0 25953
	(0001, F_2)	5(3, F_1)10	0 16967	0 16967	0 16967	0 16967	0 16967
	(0001, F_2)	6(0, A_1)10^{10}	0 4276	0 4276	0 4276	0 4276	0 4276

[a)] e r ce r m e 37

Table 5. Part of experimental line strengths, widths and shifts in the $\nu_2+\nu_4$ bands of ^{M}GeH$_4$ (M = 70, 72, 73, 74, 76)[a].

J	γ	n	J'	γ'	n'	ν^{Exp} cm^{-1}	Int$^{\mathrm{Exp}}$ cm^{-2}·atm^{-1}	δ in %	γ_{self} cm^{-1}atm^{-1}	δ_{self} cm^{-1}atm^{-1}	Band	M
1			2			3	4	5	6	7	8	9
9	A_2	10	8	A_1	1	1832.6341	0.2191E-01	4.1	6.93(17)	-6.06(49)	$\nu_2+\nu_4(F_2)$	76
9	E	19	8	E	1	1832.8964	0.8282E-02	-0.8	7.17(04)	-5.32(16)	$\nu_2+\nu_4(F_2)$	74
9	F_2	28	8	F_1	1	1832.9415	0.1236E-01	-1.7	7.03(03)	-6.08(18)	$\nu_2+\nu_4(F_2)$	74
9	A_2	10	8	A_1	1	1833.0230	0.2117E-01	0.2	7.09(01)	-5.14(17)	$\nu_2+\nu_4(F_2)$	74
9	A_2	10	8	A_1	1	1833.2250	0.2149E-01	1.5	7.20(07)	-7.91(60)	$\nu_2+\nu_4(F_2)$	73
9	E	19	8	E	1	1833.3060	0.8213E-02	-2.0	7.47(05)	-6.05(45)	$\nu_2+\nu_4(F_2)$	72
9	A_2	10	8	A_1	1	1833.4334	0.2127E-01	0.3	9.24(93)	-7.81(44)	$\nu_2+\nu_4(F_2)$	72
9	F_2	28	8	F_1	1	1833.7836	0.1259E-01	-0.6	7.41(06)	-3.95(42)	$\nu_2+\nu_4(F_2)$	70
9	A_2	10	8	A_1	1	1833.8660	0.2167E-01	1.8	7.26(03)	-7.05(13)	$\nu_2+\nu_4(F_2)$	70
15	F_2	35	14	F_1	3	1834.2135	0.1241E-02	1.5	6.79(28)	-5.64(49)	$\nu_2+\nu_4(F_1)$	74
15	F_1	37	14	F_2	4	1835.1132	0.1401E-02	-7.1	9.15(22)		$\nu_2+\nu_4(F_2)$	74
10	A_1	11	9	A_2	1	1835.7684	0.1501E-01	2.0	7.99(14)	-6.60(46)	$\nu_2+\nu_4(F_2)$	76
10	A_1	11	9	A_2	1	1836.1254	0.1491E-01	0.8	7.37(02)	-4.01(22)	$\nu_2+\nu_4(F_2)$	74
10	A_1	11	9	A_2	1	1836.3107	0.1545E-01	4.1	7.32(08)	-6.05(32)	$\nu_2+\nu_4(F_2)$	73
10	F_1	30	9	F_2	2	1836.6374	0.8229E-02	-0.8	7.55(04)	-3.87(34)	$\nu_2+\nu_4(F_2)$	74
10	F_2	30	9	F_1	3	1836.7787	0.9119E-02	5.5	8.22(27)	-4.46(51)	$\nu_2+\nu_4(F_2)$	76
10	F_1	30	9	F_2	2	1836.8241	0.7981E-02	-4.2	6.27(14)	-7.11(60)	$\nu_2+\nu_4(F_2)$	73
10	A_1	11	9	A_2	1	1836.8986	0.1522E-01	2.1	7.30(11)	-4.50(13)	$\nu_2+\nu_4(F_2)$	70
10	F_1	30	9	F_2	2	1837.0167	0.8462E-02	1.4	6.78(04)	-4.38(39)	$\nu_2+\nu_4(F_2)$	72
10	F_2	30	9	F_1	3	1837.1421	0.8424E-02	-2.9	7.44(03)	-4.66(22)	$\nu_2+\nu_4(F_2)$	74
10	F_2	30	9	F_1	3	1837.5254	0.8595E-02	-1.3	7.48(04)	-3.85(26)	$\nu_2+\nu_4(F_2)$	72
10	F_2	30	9	F_1	3	1837.9292	0.8788E-02	0.5	7.57(06)	-2.60(19)	$\nu_2+\nu_4(F_2)$	70
10	A_2	10	9	A_1	1	1838.1854	0.1620E-01	4.6	6.80(08)	-6.05(24)	$\nu_2+\nu_4(F_2)$	76
10	A_2	10	9	A_1	1	1838.5572	0.1550E-01	-0.2	7.52(03)	-4.73(20)	$\nu_2+\nu_4(F_2)$	74
10	A_2	10	9	A_1	1	1838.7503	0.1513E-01	-2.8	7.30(06)	-5.46(54)	$\nu_2+\nu_4(F_2)$	73
10	F_2	31	9	F_1	2	1838.8620	0.9477E-02	-2.0	6.62(05)	-8.06(29)	$\nu_2+\nu_4(F_2)$	76
10	A_2	10	9	A_1	1	1838.9493	0.1539E-01	-1.3	7.39(04)	-4.55(29)	$\nu_2+\nu_4(F_2)$	72
10	F_2	31	9	F_1	2	1839.2378	0.9619E-02	-1.0	7.22(01)	-5.99(15)	$\nu_2+\nu_4(F_2)$	74
10	A_2	10	9	A_1	1	1839.3627	0.1560E-01	-0.3	7.66(03)	-2.82(32)	$\nu_2+\nu_4(F_2)$	70
10	E	21	9	E	1	1839.4373	0.6454E-02	-2.3	6.77(03)	-9.85(77)	$\nu_2+\nu_4(F_2)$	74
10	E	21	9	E	1	1839.8349	0.6931E-02	4.4	6.89(05)	-4.12(36)	$\nu_2+\nu_4(F_2)$	72
10	E	21	9	E	1	1840.2541	0.6309E-02	-5.3	7.93(30)		$\nu_2+\nu_4(F_2)$	70
16	A_1	14	15	A_2	2	1841.2260	0.1812E-02	1.7	6.34(16)	-6.24(24)	$\nu_2+\nu_4(F_2)$	74
10	F_2	32	9	F_1	1	1842.3102	0.1088E-01	2.4	6.54(11)	-2.65(16)	$\nu_2+\nu_4(F_2)$	76
10	F_1	31	9	F_2	1	1842.6406	0.1057E-01	-0.6	6.94(04)	-5.90(19)	$\nu_2+\nu_4(F_2)$	74
10	F_2	32	9	F_1	1	1842.7016	0.1052E-01	-1.4	7.01(04)	-5.17(11)	$\nu_2+\nu_4(F_2)$	74
17	F_1	40	16	F_2	3	1842.7930	0.5620E-03	-0.7			$\nu_2+\nu_4(F_2)$	74
10	F_1	31	9	F_2	1	1842.8437	0.1126E-01	5.4	5.90(11)	-11.27(66)	$\nu_2+\nu_4(F_2)$	73
10	F_2	32	9	F_1	1	1842.9049	0.1091E-01	2.0	6.08(07)		$\nu_2+\nu_4(F_2)$	73
10	F_1	31	9	F_2	1	1843.0529	0.1042E-01	-2.4	7.05(05)	-7.01(19)	$\nu_2+\nu_4(F_2)$	72
10	F_2	32	9	F_1	1	1843.1144	0.1056E-01	-1.4	6.85(03)	-6.30(42)	$\nu_2+\nu_4(F_2)$	72
10	F_1	31	9	F_2	1	1843.4879	0.1058E-01	-1.2	8.20(09)	-2.88(31)	$\nu_2+\nu_4(F_2)$	70
10	F_2	32	9	F_1	1	1843.5497	0.1074E-01	-0.1	7.53(09)	-7.67(27)	$\nu_2+\nu_4(F_2)$	70
11	F_1	33	10	F_2	3	1844.6698	0.7060E-02	1.0	7.30(05)	-5.54(23)	$\nu_2+\nu_4(F_2)$	74
11	F_1	33	10	F_2	3	1844.8541	0.6822E-02	-2.6	6.74(30)	-4.74(28)	$\nu_2+\nu_4(F_2)$	73
11	E	22	10	E	2	1845.4026	0.4588E-02	2.1	7.27(06)	-4.42(34)	$\nu_2+\nu_4(F_2)$	74
11	E	22	10	E	2	1845.7808	0.4617E-02	2.2	7.08(10)	-4.78(43)	$\nu_2+\nu_4(F_2)$	72
11	F_2	33	10	F_1	2	1845.8618	0.6884E-02	-0.9	7.84(01)	-4.11(14)	$\nu_2+\nu_4(F_2)$	74
11	F_2	33	10	F_1	2	1846.0496	0.6863E-02	-1.4			$\nu_2+\nu_4(F_2)$	73
11	F_2	33	10	F_1	2	1846.2436	0.7021E-02	0.6	8.06(13)	-7.38(29)	$\nu_2+\nu_4(F_2)$	72
11	A_2	12	10	A_1	1	1846.4633	0.1309E-01	4.7	7.29(28)	-5.85(36)	$\nu_2+\nu_4(F_2)$	76
11	A_2	12	10	A_1	1	1846.8316	0.1264E-01	0.8	7.25(02)	-5.56(31)	$\nu_2+\nu_4(F_2)$	74
11	A_2	12	10	A_1	1	1847.0230	0.1296E-01	3.1	6.81(06)	-6.03(41)	$\nu_2+\nu_4(F_2)$	73

[a] Temperature is 296.75 K.

Table 6. Spectroscopic parameters $P^{(\Omega K\Gamma)}_{(v_l\Gamma_l)(v_u\Gamma_u)}$ of the effective dipole moment parameters of the $\nu_2+\nu_4$, $2\nu_2$ and $2\nu_4$ bands of the ^{M}GeH$_4$ isotopologues (in D)[a)]

$(v_l,\Gamma_l)/(v_u,\Gamma_u)$	$\Gamma^{b)}_{\rm sb}$	(Ω,K,Γ)	$M=70$	$M=72$	$M=73$	$M=74$	$M=76$
1	2	3	4	5	6	7	8
$(0000,A_1)/(0200,E)$	E	$(1,1,F_1)\times10^4$	-0.5200	-0.5200	-0.5200	-0.5200(32)	-0.5200
$(0000,A_1)/(0101,F_1)$	F_1	$(1,1,F_1)\times10^4$	-0.6932	-0.6932	-0.6932	-0.6932(38)	-0.6932
$(0000,A_1)/(0101,F_2)$	F_2	$(0,0,A_1)\times10^1$	0.175352(55)	0.175202(48)	0.175114(51)	0.175010(24)	0.174847(84)
$(0000,A_1)/(0101,F_2)$	F_2	$(1,1,F_1)\times10^3$	0.21711	0.21711	0.21711	0.21711(38)	0.21711
$(0000,A_1)/(0002,E)$	E	$(1,1,F_1)\times10^4$	-0.5219	-0.5219	-0.5219	-0.5219(25)	-0.5219
$(0000,A_1)/(0002,F_2)$	F_2	$(0,0,A_1)\times10^2$	-0.36664(25)	-0.36410(23)	-0.36290[c)]	-0.36161(64)	-0.35950[c)]
$(0000,A_1)/(0002,F_2)$	F_2	$(1,1,F_1)\times10^4$	0.9064	0.9064	0.9064	0.9064(56)	0.9064
$N^{\rm tr}/J^{\rm max}$			382/14	511/17	116/15	556/19	132/14
$d_{\rm rms}$			3.46%	3.49%	3.34%	3.42%	3.36%
$Z(296.75)$			1724.08	1724.26	1724.37	1724.46	1724.64

[a)] Values in parentheses are 1σ statistical confidence intervals. Parameters presented without confidence intervals have been constrained to the values of corresponding parameters of the ^{74}GeH$_4$ isotopologue.
[b)] $\Gamma_{\rm sb}$ is a symmetry of vibrational subband.
[c)] Parameter was constrained to the theoretically estimated values (see text for details).

References

[1] Ulenikov ON, Gromova OV, Bekhtereva ES, Raspopova NI, Fomchenko AL, Sennikov PG, Koshelev MA, Velmuzhova IA, Velmuzhov AP. First high resolution ro–vibrational study of the (0200), (0101) and (0002) vibrational states of $^{M}GeH_4$ ($M = 76, 74$). J Quant Spectrosc Radiat Transfer 2016;182:199–218.

[2] Ulenikov ON, Gromova OV, Bekhtereva ES, Raspopova NI, Koshelev MA, Velmuzhova IA, Bulanov AD, Sennikov PG. High–resolution FTIR spectroscopic study of $^{73}GeH_4$ up to 2300 cm^{-1}. J Quant Spectrosc Radiat Transfer 2018;221:129–37.

[3] Ulenikov ON, Gromova OV, Bekhtereva ES, Raspopova NI, Kuznetsov AV, Koshelev MA, Velmuzhova IA, Sennikov PG. First high–resolution comprehensive analysis of $^{72}GeH_4$ spectra in the Dyad and Pentad regions. J Quant Spectrosc Radiat Transfer 2019;225:206–213.

[4] Haller EE, Germanium: From its discovery to SiGe devices. Mater Sci Semicond Process 2006;9:408–22.

[5] Agostini M, Allardt M, Andreotti E, Bakalyarov AM, Balata M, Barabanov I, et al. The background in the $0\nu\beta\beta$ experiment GERDA. Eur Phys J 2014;74:1–25.

[6] Fink U, Larson HP, Treffers RR. Germane in the atmosphere of Jupiter. Icarus 1978;34:344–54.

[7] Kunde V, Hanel R, Maguire W, Gautier D, Baluteau J–P, Marten A, Chédin A, Husson N, Scott N. The tropospheric gas composition of the North Equatorial Belt (NH_3, PH_3, CH_3D, GeH_4, H_2O) and the Jovian D/H isotopic ratio. Astrophys J 1982;263:443–67.

[8] Drossart P, Encrenaz T, Kunde V, Hanel R, Combes M. An estimate of the PH_3, NH_3, CH_3D and GeH_4 abundances on Jupiter from the Voyager IRIS data at 4.5 μm. Icarus 1982;49:416–26.

[9] Chen F, Judge DL, Wu CYR, Caldwell J, White HP, Wagener R. High-resolution, low–temperature photoabsorption cross sections of C_2H_2, PH_3, AsH_3, and GeH_4, with application to Saturn's atmosphere. J Geophys Res 1991;96:17519–27.

[10] Atreya SK, Mahaffy PR, Niemann HB, Wong MH, Owen TC. Composition and origin of the atmosphere of Jupiter–an update, and implications for the extrasolar giant planets. Planetary and space science 2003;51:105–12.

[11] Lodders K. Jupiter formed with more tar than ice. Astrophys J 2004;611:587–97.

[12] Ulenikov ON, Sun F–G, Wang X–G, Zhu Q–S. High resolution spectroscopic study of arsine: $3\nu_1$, and $2\nu_1 + \nu_3$ dyad: The tendency of symmetry reduction. J Chem Phys 1996;105:7310–15.

[13] Ulenikov ON, Tolchenov RN, Koivusaari M, Alanko S, Anttila R. High–resolution Fourier transform spectra of CH_2D_2: Pentade of the lowest interacting vibrational bands $\nu_4(A_1)$, $\nu_7(B_1)$, $\nu_9(B_2)$, $\nu_5(A_2)$, and $\nu_3(A_1)$. J Mol Spectrosc 1994;167:109–30.

[14] Ulenikov ON, Burger H, Jerzembeck W, Onopenko GA, Bekhtereva ES, Petrunina OL. The ground vibrational states of PH_2D and PHD_2. J Mol Struct 2001;599:225–37.

[15] Ulenikov ON, Liu A–W, Bekhtereva ES, Gromova OV, Hao L–Y, Hu S–M. High–resolution Fourier transform spectrum of H_2S in the region of the second hexade. J Mol Spectrosc 2005;234:270–8.

[16] Ulenikov ON, Gromova OV, Bekhtereva ES, Maul C, Bauerecker S, Gabona MG, Tan TL. High resolution ro–vibrational analysis of interacting bands ν_4, ν_7, ν_{10}, and ν_{12}, of $^{13}C_2H_4$. J Quant Spectrosc Radiat Transfer 2015;151:224–38.

[17] Kagann RH, Ozier I, McRae GA, Gerry MCL. The distortion moment spectrum of GeH_4: the microwave Q branch. Can J Phys 1979;57:593–600.

[18] Daunt SJ, Halsey GW, Fox K, Lovell RJ, Gailar NM. High–resolution infrared spectra of ν_3 and $2\nu_3$ of germane. J Chem Phys 1978;68:1319–21.

[19] Fox K, Halsey GW, Daunt SJ, Kennedy RC. Transition moment for ν_3 of $^{74}GeH_4$. J Chem Phys 1979;70:5326–7.

[20] Kreiner WA, Magerl G, Furch B, Bonek E. IR laser sideband observations in GeH_4 and CD_4. J Chem Phys 1979;70:5016–20.

[21] Magerl G, Schupita W, Bonek E, Kreiner WA. Observation of the isotope effect in the ν_2 fundamental of germane. J Chem Phys 1980;72:395–8.

[22] Kreiner WA, Opferkuch R, Robiette AG, Turner PH. The ground-state rotational constants of Germane. J Mol Spectrosc 1981;85:442–8.

[23] Lepage P, Champion JP, Robiette AG. Analysis of the ν_3 and ν_1 infrared bands of GeH_4. J Mol Spectrosc 1981;89:440–8

[24] Schaeffer RD, Lovejoy RW. Absolute line strengths of $^{74}GeH_4$ near 5 μm. J Mol Spectrosc 1985;113:310–4.

[25] Zhu Q, Thrush BA, Robiette AG. Local mode rotational structure in the (3000) Ge-H stretching overtone ("$3\nu_3$") of germane. Chem Phys Lett 1988;150:181–3.

[26] Zhu Q, Thrush BA. Rotational structure near the local mode limit in the (3000) band of germane. J Chem Phys 1990;92:2691–7.

[27] Zhu Q, Qian H, Thrush BA. Rotational analysis of the (2000) and (3000) bands and vibration-rotation interaction in germane local mode states. Chem Phys Lett 1991;186:436–40.

[28] Campargue A, Vetterhöffer J, Chenevier M. Rotationally resolved overtone transitions of $^{70}GeH_4$ in the visible and near-infrared. Chem Phys Lett 1992;192:353–6.

[29] Zhu Q, Campargue A, Vetterhöffer J, Permogorov D, Stoeckel F. High resolution spectra of GeH_4 v = 6 and 7 stretch overtones. The perturbed local mode vibrational states. J Chem Phys 1993;99:2359–64.

[30] Sun F, Wang X, Liao J, Zhu Q. The (5000) Local Mode Vibrational State of Germane: A high-resolution spectroscopic study. J Mol Spectrosc 1997;184:12–21.

[31] Chen XY, Lin H, Wang XG, Deng K, Zhu QS. High–resolution Fourier transform spectrum of the (4000) local mode overtone of GeH_4: local mode effect. J Mol Struct 2000;517–518:41–51.

[32] Boudon V, Grigoryan T, Philipot F, Richard C, Kwabia Tchana F, Manceron L, Rizopoulos A, Vander Auwera J, Encrenaz T. Line positions and intensities for the ν_3 band of 5 isotopologues of germane for planetary applications. J Quant Spectrosc Radiat Transfer 2018;205:174–83.

[33] Richard C, Boudon V, Rotger M. Calculated spectroscopic databases for the VAMDC portal: New molecules and improvements. J Quant Spectrosc Radiat Transfer 2020;251:107096.

[34] Bretherick's Handbook of Reactive Chemical Hazards, Peter Urban, edt., 8th edition, Elsevier 2017, 2680 p.

[35] Ulenikov ON, Gromova OV, Bekhtereva ES, Raspopova NI, Sydow C, Bauerecker S. Line strengths analysis of germane in the 1100–1350 cm^{-1} region: the $\nu_1 - \nu_4$, $\nu_3 - \nu_4$, $\nu_3 - \nu_2$ and $\nu_1 - \nu_2$ "hot" bands of $^M GeH_4$ ($M = 70, 72, 73, 74, 76$). J Quant Spectrosc Radiat Transfer 2020;242:106755.

[36] Albert S, Albert–Keppler K, Quack M. Handbook of high–resolution spectroscopy, 2. Chichester, NY: John Wiley & Sons, Ltd; 2011. p. 965–1019.

[37] Ulenikov ON, Gromova OV, Bekhtereva ES, Raspopova NI, Kuznetsov AV, Sydow C, Bauerecker S. High resolution analysis of GeH_4 in the dyad region:

Ro–vibration energy structure of $^{70}GeH_4$ and line strengths of $^{M}GeH_4(M = 70, 72, 73, 74, 76)$. J Quant Spectrosc Radiat Transfer 2019;236:106581.

[38] Fano U, Racah G. Irreducible tensorial sets. New York: Academic Press; 1959.

[39] Wigner EP. Group theory and its application to the quantum mechanics of atomic spectra. New York–London: Academic Press; 1959.

[40] Hecht K. The vibration–rotation energies of tetrahedral XY_4 molecules. J Mol Spectrosc 1960;5:355–89.

[41] Moret-Bailly J. Sur l'interpretation des spectres de vibration-rotation des molecules a symmetrie tetraedrique ou octaedrique. Cah Phys 1961;15:237–314.

[42] Champion J–P, Pierre G, Michelot F, Moret-Bailly J. Composantes cubiques normales des tenseurs spheriques. Can J Phys 1977;55:512-20.

[43] Moret-Bailly J, Gautier L, Montagutelli J. Clebsch–Gordan coefficients adapted to cubic symmetry. J Mol Spectrosc 1965;15:355–77.

[44] Rey M, Boudon V, Wenger Ch, Pierre G, Sartakhov B. Orientation of O(3) and SU(2)$\otimes C_I$ representation in cubic point groups (O_h, T_d) for application to molecular spectroscopy. J Mol Spectrosc 2003;219:313–25.

[45] Wenger C, Boudon V, Rotger M, Sanzharov N, Champion J–P. XTDS and SPVIEW: Graphical tools for the analysis and simulation of high–resolution molecular spectra. J Mol Spectrosc 2008;251:102–13.

[46] Koshelev MA, Velmuzhov AP, Velmuzhova IA, Sennikov PG, Raspopova NI, Bekhtereva ES, Gromova OV, Ulenikov ON. High resolution study of strongly interacting $\nu_1(A_1)/\nu_3(F_2)$ bands of $^{M}GeH_4$ ($M = 76, 74$). J Quant Spectrosc Radiat Transfer 2015;164:161–74.

[47] Bykov AD, Makushkin YuS, Ulenikov ON. On isotope effect in polyatomic molecules. Some comments on the method. J Mol Spectrosc 1981;85:462–79.

[48] Loéte M. Développement complet du moment dipolaire des molécules tétraédriques. Application aux bandes triplement dégénérées et à la diade ν_2 et ν_4. Can J Phys 1983;61:1242–59.

[49] Saveliev VN, Ulenikov ON. Calculation of vibration–rotation line intensities of polyatomic molecules based on the formalism of irreducible tensorial sets. J Phys B: At Mol Phys 1987;20:67–83.

[50] Flaud JM, Camy-Peyret C. Vibration–rotation intensities in H_2O–type molecules application to the $2\nu_2$, ν_1, ν_3 band of $H_2^{16}O$. J Mol Spectrosc 1975;55:278–310.

[51] Herzberg G. Molecular spectra and molecular structure. Infrared and Raman spectra of polyatomic molecules. vol. 2. New York: van Nostrand; 1945.

[52] Fox K. On the rotational partition function for tetrahedral molecules. J Quant Spectrosc Radiat Transfer 1970;10:1335–42.

[53] Griffits DJ. Introduction to quantum mechanics. New Jersey: Prentice Hall, Inc.; 1995.

[54] Schmitt M, Meerts L. Structures and Dipole moments of molecules in their electronically excited states. In: Laane J, editor. Frontiers and advances in molecular spectroscopy. Amsterdam: Elsevier; 2018. p. 143–93.

[55] Varshalovitch DA, Moskalev AN, Khersonsky VK. Quantum theory of angular momentum. Leningrad: Nauka; 1975.

[56] Nielsen HH. The vibration–rotation energies of molecules. Rev Mod Phys 1951;23:90–136.

[57] Papousek D, Aliev MR. Molecular vibrational–rotational spectra. Amsterdam: Elsevier; 1982.

[58] Amat G, Goldsmith M, Nielsen HH. Higher order rotation–vibration energies of polyatomic molecules. I. J Chem Phys 1956;24:1178–86.

[59] Amat G, Goldsmith M, Nielsen HH. Higher order rotation–vibration energies of polyatomic molecules. II. J Chem Phys 1957;27:838–44.

[60] Amat G, Goldsmith M, Nielsen HH. Higher order rotation–vibration energies of polyatomic molecules. III. J Chem Phys 1957;27:845–50.

[61] Amat G, Nielsen HH. Higher order rotation–vibration energies of polyatomic molecules. IV. J Chem Phys 1958;29:665–72.

[62] Amat G, Nielsen HH. Higher order rotation–vibration energies of polyatomic molecules. V. J Chem Phys 1962;36:1859–65.

[63] Amat G, Nielsen HH, Tarrago G. Rotation–vibration of polyatomic molecules. New–York: M.Dekker, Inc.; 1971.

[64] Jorgensen F, Pedersen T. A projector formulation for the Van Vleck transformation. I. Degenerate case. Mol Phys 1974;27:33–47.

[65] Jorgensen F. Effective hamiltonians. Mol Phys 1975;29:1137–64.

[66] Jorgensen F, Pedersen T, Chedin A. A projector formulation for the Van Vleck transformation. III. Generalization and relation to the contact transformation Mol Phys 1975;30:1377–95.

[67] Cheglokov AE, Ulenikov ON, Zhilyakov AS, Cherepanov VN, Makushkin YuS, Malikova AB. On the determination of spectroscopic constants as functions of intramolecular parameters. J Phys B: At Mol Opt Phys 1989;22:997–1015.

[68] Champion JP. Developpement complet de l'hamiltonien de vibration–rotation adapte a l'etude des interactions dans les molecules toupies spheriques. Application aux bandes ν_2 et ν_4 de $^{12}CH_4$. Can J Phys 1977;55:1802–28.

[69] Zhilinskii BI. Method of irreducible tensorial sets in molecular spectroscopy (in Russian), Moscow State University Press, Moscow, 1981.

[70] Boudon V, Champion JP, Gabard T, Loëte M, Rotger M, Wenger C. Spherical top theory and molecular spectra. In: Quack M, Merkt F, editors. Handbook of high–resolution spectroscopy, vol.3. Wiley; 2011.p.1437–60.

[71] Fano U,Racah G. Irreducible tensorial sets. NewYork: Academic Press; 1959.

[72] Wigner EP. Quantum theory of angular momentum. NewYork: Academic Press; 1965.

[73] Silver BL. Irreducible tensorial methods. New York–London: Academic Press; 1976.

[74] Moret-Bailly J, Gautier L, Montagutelli J. Clebsch-Gordan coefficients adapted to cubic symmetry. J Mol Spectrosc 1965;15:355–77.

[75] Sviridov DT, Sviridova RK, Smirnov YuF. Optical Spectra of Transition Metal Ions in Cristals. Moscow: Nauka; 1976.

[76] Davis SP, Abrams MC, Brault JW. Fourier transform spectrometry. San Diego: Academic Press; 2001.

[77] Tran H, Ngo NH, Hartmann J–M. Efficient computation of some speed–dependent isolated line profiles. J Quant Spectrosc Radiat Transfer 2013;129:199–203.

[78] Tran H, Ngo NH, Hartmann J–M, Gamache RR, Mondelain D, et al. Velocity effects on the shape of pure H_2O isolated lines: complementary tests of the partially correlated speed–dependent Keilson–Storer model. J Chem Phys 2013;138:034302.

[79] Tennyson J, Bernath PF, Campargue A, Csaszar AG, Daumont L, Gamache RR. Recommended isolated–line profile for representing high–resolution spectroscopic transitions (IUPAC technical report). Pure Appl Chem 2014;86:1931–43.

[80] Nelkin M, Ghatak A. Simple binary collision model for Van Hove's $G_e(r,t)$. Phys Rev 1964; 135(1A): A4–9.

[81] Humlicek J. Optimized computation of the Voigt and complex probability functions. J Quant Spectrosc Radiat Transf 1982;27(4),437–44.

[82] Armstrong BH. Spectrum line profiles: the Voigt function. J Quant Spectrosc Radtat Transfer 1967;7:61–88.

[83] Lether FG, Wenston PR. The numerical computation of the Voigt function by a corrected midpoint quadrature rule. J Comput Appl Math 1991;34:75–92.

[84] Rautian SG, Sobelman II. The effect of collisions on the Doppler broadening of spectral lines. Soviet Phys Usp 1967;9:701–16.

[85] Berman PR. Speed–dependent collisional width and shift parameters in spectral profiles. J Quant Spectrosc Radiat Transf 1972;12:1331–42.

[86] Pickett HM. Effects of velocity averaging on the shapes of absorption lines. J Chem Phys 1980;73:6090–4.

[87] Lance B, Blanquet G, Walrand J, Bouanich J. On the speed–dependent hard collision lineshape models: application to C_2H_2 Perturbed by Xe. J Mol Spectrosc 1997;185:262–71.

[88] Galatry L. Simultaneous effect of Doppler and foreign gas broadening on spectral lines. Phys Rev 1961;122:1218–1223.

[89] Boone CD, Walker KA, Bernath PF. J Quant Spectrosc Radiat Transf 2007;105:525–32.

[90] Dicke RH. The effect of collisions upon the Doppler width of spectral lines. Phys Rev 1953;89:472–3.

[91] Murray JR and Javan A. Effects of collisions on Raman line profiles of hydrogen and deuterium gas. J Mol Spectrosc 1972;42:1–26.

[92] Eng RS, Calawa AR, Harman TC, Kelley PL, and Javan A. Collisional narrowing of infrared water vapor transitions. Appl Phys Lett 1972;21:303–5.

[93] Pine AS. Collisional narrowing of HF fundamental band spectral lines by neon and argon. J Mol Spectrosc 1980;82:435–48.

[94] Varghese PL, Hanson RK. Collisional narrowing effects on spectral line shapes measured at high resolution. Appl Opt 1984;23:2376–85.

[95] Ng EW, Geller M. A table of integrals of the error functions. J Res NBS: B Math Sci 1969;73B:1–20.

[96] Andrews LC. Special functions of mathematics for engineers. Oxford: SPIE Press; 1998.

O. N. Ulenikov: Conceptualization, Supervision, Writing - Review & Editing, Methodology, Investigation, Writing - Original Draft

E. S. Bekhtereva: Methodology, Software, Investigation

O. V. Gromova: Methodology, Software, Investigation

N. I. Raspopova: Validation, Investigation

A. V. Kuznetsov: Validation, Investigation

V. Boudon Methodology, Software, Investigation

K. B. Berezkin: Validation, Investigation, Resources

C. Sydow: Validation, Investigation, Resources

S. Bauerecker: Validation, Investigation, Resources, Conceptualization, Supervision

Declaration of Competing Interest

There are no conflicts to declare.